Zimmermann, G., Zang, A., Stephansson, O., Klee, G., Semikova, H. (2019): Permeability Enhancement and Fracture Development of Hydraulic In Situ Experiments in the Äspö Hard Rock Laboratory, Sweden. - *Rock Mechanics and Rock Engineering*, *52*, 2, pp. 495—515.

DOI: http://doi.org/10.1007/s00603-018-1499-9

Permeability enhancement and fracture development of hydraulic in-situ experiments in the Äspö Hard Rock Laboratory, Sweden

Authors: Günter Zimmermann[1*], Arno Zang[1], Ove Stephansson[1], Gerd Klee[2], Hana Semiková[3]

[1] Helmholtz-Zentrum Potsdam - Deutsches GeoForschungsZentrum GFZ, Telegrafenberg, D-14473 Potsdam, Germany

[2] MeSy-Solexperts GmbH, Meesmannstr. 49, D-44807 Bochum, Germany

[3] ISATech s.r.o., Osadní 26, Prague 7, 170 00, Czech Republic

[*] Corresponding author: Günter Zimmermann
E-mail address: guenter.zimmermann@gfz-potsdam.de
Tel: +49 331 288 1458

Abstract

A new advanced protocol of progressively increased cyclic injection and pulsed injection design for hydraulic fracturing experiments was implemented at 410 m depth in the Äspö Hard Rock Laboratory in Sweden. A monitoring array was installed around the tested horizontal borehole to detect the acoustic emissions and micro-seismic events during the fracturing process. The aim is to identify optimised injection schemes to reduce the seismicity related to the fracturing processes. The cyclic stimulation scheme of loading and unloading the fracturing net pressure leads to a lower accompanied seismicity if compared to the conventional hydraulic fracturing with constant flow rates. The related permeability of the tested rock interval can be increased, but this increase is less pronounced than that of the conventional treatments and, especially, if compared to the last of the re-fracturing series with high seismicity increase. Despite these limitations, in field applications with expected high risk of unwanted seismic events, this advanced protocol can be a feasible option to reduce this risk.

Keywords: hydraulic fracturing; cyclic stimulation; pulsed stimulation; fatigue stimulation concepts; Äspö HRL

Abbreviations

AE	Acoustic emission
EGS	Enhanced geothermal system
EM	Electromagnetic
FBP	Formation breakdown pressure
HF	Hydrofracturing test
HRL	Hard rock laboratory
ISIP	Instantaneous shut-in pressure
M	Monitoring borehole
MF	Main frac
MS	Micro seismic
RF	Refrac cycle

RFP	Refrac pressure
S1	Maximum principal stress
S2	Intermediate principal stress
S3	Minimum principal stress
Sh	Minimum horizontal stress
h	Interval length
k	Permeability
ln	Natural logarithm
q	Flow rate
q_{mean}	Mean flow rate
t_0	Injection time
Δt	Shut-in time
V_{inj}	Fluid volume injected
V_{re}	Fluid volume returned
α	Dip (with respect to horizontal)
β	Dip direction (North over East)
θ	Fracture strike direction (North over East)
μ	Dynamic viscosity of fluid

1 Introduction

In general, hydraulic stimulation can be described as injection of fluids at high flow rates into reservoirs to develop new fractures or reactivate existing fractures. The aim is to enhance the productivity of low permeability rock for extraction of hydrocarbons or energy extraction for geothermal use. In geothermal applications these stimulation treatments are required to develop suitable heat exchangers to extract economic amounts of heat and are referred to as Enhanced Geothermal Systems (EGS) (Tester et al. 2006).

The basic concepts of hydraulic stimulation include different processes of fracture initiation and propagation (e.g. Economides and Nolte 2000). This can be summarized by different failure criteria (e.g. Zang and Stephansson 2010) and loading modes (e.g. Shen et al. 2014), i.e. tensile failure (mode I), failure in shear (mode II) or tearing (or out-of plane shearing) mode (mode III). The most efficient way regarding the effectiveness of generating new pathways for fluids to enhance permeability is hydraulic shearing since the fractures keep residual conductivity after pressure release (the so called self-propping effect). In contrast, pure tensile fracturing, where the developed fractures can completely close after the pressure is released, is less efficient. In the case of pure tensile fracturing the opening of fractures is typically supported by placing of proppants (e.g. Schubarth and Milton-Tayler 2004; Deon et al. 2013; Reinicke et al. 2013; Palisch et al. 2015), which are transported via high viscosity gels into the formation (e.g. Johnson et al. 1993; Legarth et al. 2005; Zimmermann and Reinicke 2010).

The stimulation treatments are usually accompanied by seismic events, mainly resulting from a failure in shear if high magnitudes are concerned. In some cases of geothermal site development the projects had to be suspended such as in Basel, Switzerland, due to damages from earthquakes during the injection and subsequent shut-in of the well. In this case expected further high environmental risks from induced seismicity during later stages of the project led to the suspension of the project (Häring et al. 2008).

The general aim of stimulation is to develop an advanced injection strategy to control the fracture propagation and simultaneously reduce the risks of unwanted seismic events beyond a certain threshold depending on the vulnerability and exposure of people, buildings and infrastructure (Majer et al. 2007). In this context many efforts have been made to develop stimulation concepts to mitigate the risk of unwanted high seismicity and simultaneously enhance the permeability of the rock. One option to optimize the development of fracture networks based on hydraulic fracturing treatments is a cyclic injection scheme. An early study applying a cyclic stimulation scheme was done by Kiel (1977) to develop long and branching fractures in natural fractured formations in US petroleum basins. He named this treatment dendritic fracturing, and it resulted in a much higher productivity enhancement compared to conventional hydraulic treatments. The scheme includes an alternation of injection stages and shut-in or flow back (also called bleed off), and the basic idea behind this is a relaxing process by reducing the fracture net pressure after each injection stage. He argued that this causes the production of spalls from the asperities of the fracture faces, which can then act as proppants and increase the fracture conductivity. Subsequent stages result in spalling and branching of secondary fractures. Seismicity was not considered in this study by Kiel (1977).

A similar cyclic treatment was carried out in a geothermal well and resulted in low seismicity, which was monitored by a down-hole geophone in a neighbouring well (Zimmermann et al. 2010; Kwiatek et al. 2010). The main difference compared to the Kiel (1977) approach was to perform the treatment without a shut-in and having instead low flow rate stages to keep the fracture open. In addition, the scheme included the transport of meshed quartz sand during the high flow rates. The main purpose of this cyclic stimulation scheme was not the reduction of seismicity but to increase the effectiveness of fracture development and placement of quartz sand during the high flow rates to keep the fractures open after pressure release and thereby increase permeability. The low seismicity was therefore a positive side effect, which can possibly be attributed to the relaxation of the fracture during the low flow rate stages similar to the approach of Kiel (1977).

According to a modelling and experimental study of Zang et al. (2013) a cyclic mechanical and cyclic hydraulic fracturing treatment results in a lower seismicity and a reduction of the number of events if compared to a conventional protocol. They argued that the loading cycles fatigues the rock by frequent lowering of the crack tip stresses, i.e. the loading is interrupted with multiple stopping phases without any further deformation (crack-rate controlled tests (Zang et al 2002)) resulting in a more narrow zone of tensile and shear fractures and hence more persistent fracture growth (Zang et al. 2000). The fracture network can be designed depending on the hydraulic cycles. A detailed description of the concept of fatigue hydraulic fracturing and its geothermal application is discussed in Zang et al. (2017b; 2018). Similar studies with a more sophisticated geometry to simulate a multi-stage fracturing design (Yoon et al. 2015a), the stress shadowing effect (Yoon et al. 2015b) and the presence of a nearby fault (Yoon et al. 2015c) confirm the findings of Zang et al. (2013).

Results of recent laboratory experiments revealed the advantages of cyclic injection (Zhuang et al. 2016, 2017) on breakdown pressure conditions of Pocheon granites. They showed that the average breakdown pressure can be reduced to a value approximately 80 % of the value of the conventional continuous injection. Another recent study was performed by Patel et al. (2017) on Tennessee sandstones under tri-axial stress conditions. They observed a

reduction of breakdown pressure by 16 % for dry specimens but no effect for saturated sandstones. They also showed that the process zone from the cyclic injection, i.e. the stimulated volume, is twice that of the conventional injection and is accompanied by an increase of acoustic events.

2 Experimental setup

The experiments were performed in the Äspö Hard Rock Laboratory (HRL), located in the south of Sweden approximately 35 km north of the city of Oskarshamm. The experimental setup and the injection schedules are described in detail in Zang et al. (2017a), therefore we only briefly recapitulate the setup and refer to the publication of Zang et al. (2017a).

The experiments were performed in the tunnel TASN in a new drilled horizontal borehole F1 at a depth level of 410 m below surface (Figure 1). In total six fracturing experiments were performed in this horizontal well drilled in the direction of minimum horizontal principal stress based on findings in a previous work by Klee and Rummel (2002) and an extensive stress evaluation by Ask (2003, 2006a, b). Two companies were involved with different test equipment and procedures. MeSy-Solexperts (Bochum, Germany) performed one multi-stage fracturing test with progressively increasing injection flow rate and two conventional hydrofracturing tests for comparison. ISATech (Prague, Czech Republic) performed a dynamic pulse test and two conventional hydrofracturing tests for comparison. The hydraulic tests were accompanied by an extensive monitoring network of acoustic emission (AE), micro seismic (MS) and electromagnetic (EM) sensors (Zang et al., 2017a).

Figure 1 Location and the high frequency seismic network of the experiment in the tunnel TASN. F1 is the location of the horizontal borehole to perform the experiments. The locations of the six hydraulic experiments are marked and are numbered in light blue. M1 to M3 are the boreholes where the AE sensors and the accelerometers were installed (red and orange colored dots). The remaining sensors and accelerometers were installed in short boreholes in the roof of surrounding tunnels (light blue, green and black colored dots). This monitoring is complemented with an electromagnetic array to observe electromagnetic emission (colored purple triangles) and self potential (blue colored dots).

The horizontal borehole F1 has a diameter of 102 mm and a length of 28 m. The high frequency seismic network consists of eleven acoustic emission (AE) sensors (Figure 1, red colored dots, frequency 1-100 kHz) and four accelerometers (Figure 1, orange colored dots, frequency below 25 kHz). The AE sensors were placed in three monitoring boreholes located left and right of the hydraulic testing borehole (M1, M2 and M3). The remaining AE sensors and accelerometers were installed in short boreholes in the roof of the surrounding tunnels (light blue, green and black colored dots). This monitoring design allows us to follow hydraulic fracture propagation (perpendicular to the minimum principal stress Sh), which is the direction towards the monitoring boreholes M1, M2 and M3. The electromagnetic (EM) array involved monitoring of electromagnetic emission (purple colored triangles) and self potential (blue colored dots). A second triggered and continuous recording system was in operation at 1 MHz sampling rate. This made real-time tracking of the hydraulic fracture growth process (Kwiatek

et al. 2017) possible, as well as post processing of full waveforms (Lopez Comino et al. 2017a, b) for source analysis.

In this work we mainly focus on the permeability development and the related micro seismicity based on the fracturing processes of the different fluid injection protocols.

3 Hydraulic testing procedures

The setup of the hydraulic testing equipment is shown in Figure 2. The equipment consists of two packer elements to isolate the test interval, which can be moved by a steel tubing to the different depth sections in the borehole. The test intervals were selected after inspection with a high-resolution camera and observation of the drill cores to assure that no preexisting fractures are present. The images from the core box (Figure 3, left) and from borehole camera inspection (Figure 3, right) of the tested interval HF1 demonstrate that no fractures are visible in this test interval. After hydraulic testing, impression packer tests were performed in each interval to visualize the generation of a new fracture and to obtain the fracture orientation (see Appendix B).

Figure 2 Setup of the experiment by Mesy-Solexperts. The system consists of a packer system, which can be moved by a steel tubing to different depth sections of the borehole F1. A high pressure pump provided the interval pressure.

Figure 3 Image of the core box (left) and the camera inspection (right) of the tested interval for HF1. The chosen interval is marked in blue and demonstrates that the interval is devoid of fractures.

Three different hydraulic testing procedures were performed. First, conventional testing procedures with constant flow rates were carried out. For the second testing design, the flow rate was progressively increased. For the third procedure, an additional pressure pulse was added (see schematics in Figure 4).

Figure 4 Schematics of the different testing procedures showing flow rates (blue) and corresponding interval pressures (red). Top: conventional hydraulic fracturing procedure with constant flow rate displaying the main frac and the subsequent refrac. Middle: progressively increasing flow rate with a shut-in between cycles. The pressure is increased in steps of approximately 20 % of the expected breakdown pressure estimated from the previous conventional test in the same rock type. Bottom: progressively increasing flow rate with pressure pulses from a second pump system.

The testing procedure for the conventional hydrofracturing (HF) closely followed the recommendations of the International Society of Rock Mechanics (ISRM) for stress measurements (Haimson and Cornet 2003). The testing interval length of the MeSy-Solexperts' equipment was modified from 0.75 m to 0.5 m interval length. After inflation of the packers the conventional HF-test started with a rapid pressurization of the test interval to a pressure of up to 3 MPa and a subsequent monitoring of the pressure decline for approximately 10 minutes to test the system for potential leakage. During the main test the interval was pressurized applying a constant flow rate. Pressure was

increased until the formation breakdown pressure (FBP) was reached, followed by a decline to a stable pressure level. Subsequently the interval was shut-in and the pressure dropped instantaneously to the ISIP (instantaneous shut-in pressure) followed by a decline curve. Finally the interval pressure was released and fluid recovery was metered. This procedure was repeated several times with various flow rates to obtain the fracture reopening or refrac pressure (RFP) and in addition to observe the development of the fracture permeability.

The progressively increasing pressure design is a modification of the previous test design (see Figure 4b). In the first stage the pressure was increased to approximately 20 % of the expected formation breakdown pressure estimated from the results of the previous conventional testing. After shut-in and pressure decline for a few minutes the pressure was increased by 10 % - 20 % for each following stage (see pressure curve in Figure 4b) until a pressure drop was indicating the start of rock failure. Thereafter, four refrac cycles were performed similar to those of the conventional testing procedure for comparison.

In another series of fracturing tests a pulsed HF test and two conventional HF tests were performed in the same horizontal well by ISATech. The testing interval in this test series was reduced to 0.25 m. For the pulse testing an additional pump was used with adjustable pressure amplitude and a frequency of 5 - 6 Hz together with linear pressure pulses (see pressure curve in Figure 4c). The pressure of the linear pressure pulses was stepwise increased similar to the previous progressively increasing pressure design with a subsequent pressure release between the stages.

4 Results

The evolution of transmissivity and permeability is calculated from decline pressure curves after each injection stage according to classical well test analysis (e.g. Horne 1995 and Appendix A). The calculations based on the slope of the decline curves are performed for the last 100 seconds of each shut-in period for the conventional treatment and for the last 40 seconds for the cyclic stages. This ensures that stable and comparable radial flow conditions for each stage are obtained. The time difference is due to the fact that the shut-in time for the conventional treatments is in the range of 300-700 seconds and for the cyclic stages it is in the range of 120-130 seconds (see Table 1).

4.1 Conventional hydrofrac test HF1

The first test was the conventional hydrofrac HF1 and was performed in Ävrö Granodiorite at 25 m depth of the horizontal borehole F1 (Figure 5). The pressure versus time curve of the main fracturing cycle shows the initiation of a fracture with a distinct breakdown event at 13.1 MPa followed by a decline curve after shut-in (Figure 6). The

refrac or reopening pressure was determined from the first refrac cycle at 8.9 MPa. Subsequent refrac-cycles yielded distinct shut-in pressure values to obtain the minimum principal stress. Taking the average of all cycles yields a minimum principal stress of 8.3 MPa (Table 1).

The decline curve analysis reveals a stepwise increasing trend of permeability development in the tested interval accompanied with an increase of seismic events (Table 1). Refrac-cycle no. 4 (RF 4) shows a lower number of events due to the shorter injection time compared to the other RFs. The highest permeability increase happened during the last refrac RF5 with an increase of permeability to 7.1 mD from 1.6 mD and 1.4 mD in the previous stages RF3 and RF4. The total increase of permeability of RF5 is 12.5 times the permeability of the main frac treatment (Figure 7).

Figure 5 Chronological sequence of the conventional hydraulic fracturing experiment HF1 in Ävrö Granodiorite at 25 m depth of borehole F1. Displayed is the flow rate (blue), the interval pressure (red) and the seismic events (red dots) of the main frac (MF) and subsequent five refrac-cycles (RF1 to RF5).

Figure 6 Main frac and first refrac (RF1) of the conventional hydraulic fracturing experiment HF1 at 25 m depth of borehole F1. Displayed is the flow rate and the interval pressure; the arrows mark the formation breakdown pressure (FBP = 13.1 MPa) and the refrac pressure (RFP = 8.9 MPa) of the first refrac cycle (RF).

Figure 7 Permeability development of the conventional fracturing experiment HF1 (black colored squares and black curve, left axis). For comparison, pressure and seismic events of the different cycles are also displayed (red curve and red colored dots, right axis). The highest permeability increase happened during the fifth refrac cycle (RF5) and increased the permeability by a factor of 12.5 to 7.1 mD compared to the permeability of the main frac (MF) (0.57 mD).

Table 1 Results of the first conventional hydraulic fracturing experiment HF1 at 25 m depth in borehole F1

The recovered volume V_{re}, i.e. the flow back after pressure release, is approximately 50 % of the injected volume $V_{inj.}$ for each stage (Table 1). The related acoustic events of each stage are proportional to the injected volume.

4.2 Conventional hydrofrac test HF2

The second hydrofrac test was operated again as a conventional test with a similar schedule as HF1 and was carried out at 22.5 m depth in the same rock type Ävrö Granodiorite. The test includes the main frac followed by 5 refrac stages (Figure 8). The main frac is characterized by the initiation of a fracture with a distinct breakdown event at 10.9 MPa (Figure 9). Refrac pressure is determined from first RF and yielded 6.7 MPa. The minimum principal stress is determined from the instantaneous shut-in pressure (ISIP) of the refrac stages and yielded 8.6 MPa.

The permeability of each stage is calculated from the decline curves and shows the same trend as for HF1 with an increase of permeability (Table 2). The permeability is increased from 1.32 mD after the main frac to 3.63 mD for the first RF, whereas between RF2 and RF4 permeability keeps approximately constant. Only in the last stage RF5 permeability is increased again and accompanied with an increase of seismic events (Figure 10).

Figure 8 Chronological sequence of the conventional hydraulic fracturing experiment HF2 of Ävrö Granodiorite at 22.5 m depth in borehole F1. Displayed is the flow rate, the interval pressure and the seismic events of the main frac (MF) and subsequent five refracs (RF1 to RF5). Notice the increase of seismicity with increasing flow rate.

Figure 9 Main frac and first refrac (RF1) of the conventional hydraulic fracturing experiment HF2 at 22.5 m depth of borehole F1. Displayed is the flow rate and the interval pressure; the arrows mark the formation breakdown pressure (FBP = 10.9 MPa) and the refrac pressure (RFP = 6.7 MPa) of the first refrac cycle (RF).

Figure 10 Permeability development of the conventional fracturing experiment HF2 (black colored squares and black curve, left axis). For comparison, pressure and seismic events of the different cycles are also displayed (red curve and red colored dots, right axis). The permeability is increased from 1.32 mD after the main frac (MF) to 3.63 mD after the first refrac cycle (RF1) and stays approximately constant during the next three stages. Only in the last stage RF5 permeability is again increased to 4.78 mD.

Table 2 Results of the second conventional hydraulic fracturing experiment HF2 at 22.5 m depth in borehole F1

In contrast to the previous test HF1 the recovered volume is slightly less for HF2 and in total only 40 % of the injected volume was retrieved (Table 2). This can be due to a hydraulic communication between HF2 and HF1 as stated in Zang et al. (2017a). The number of acoustic events is again proportional to the injected volume and as well to the recovered volume.

4.3 Hydrofrac test with progressively increased flow rate HF3

This test is the specifically modified hydraulic fracturing procedure with progressively increasing pressures as described in the previous section. The test was performed at 19 m depth with an interval length of 0.5 m in the same rock type as for the two previous tests (Ävrö Granodiorite) to compare the outcome of this special test procedure to the conventional hydraulic fracturing tests. The complete chronological sequence of the test including the four refrac cycles is displayed in Figure 11. The duration of each stage of progressively increasing pressure is much shorter with 6.8 to 16 seconds compared to those for the conventional treatment, the same holds for the shut-in time between the stages with durations of approximately 130 seconds (Figure 12). The first stage started with approximately 20% of the expected formation breakdown pressure (FBP) obtained from HF1 and is stepwise increased by additional 15 % - 20 % during each cycle until formation breakdown (numbers 1 to 5 in Figure 12). The formation breakdown pressure was determined to be 9.2 MPa, which is approximately 30 % and 16 % lower

than the FBP for the conventional hydrofracs HF1 (FBP = 13.1 MPa) and HF2 (FBP = 10.9 MPa) in similar environments.

Permeability development starts with 0.2 mD for the first cycle and keeps on this level for cycle 2 and 3. During the 4th cycle it increased to 0.5 mD and kept about constant during the 5th cycle (Table 3). At this stage the hydrofrac is not accompanied with any seismicity and even during the following conventional refracs RF1 and RF2 no seismicity was detected although the permeability increased to 0.8 mD and 1.2 mD respectively (Figure 13). During RF3 one event was registered, only the last RF4 shows more seismicity with 15 registered events associated with an increase of permeability to nearly 2 mD (Table 3).

Figure 11 Complete chronological sequence of the HF3 experiment at 19 m depth in borehole F1 with progressively increasing flow rate cycles (details in Figure 12). Displayed is the flow rate (blue curve), the interval pressure (red curve) and the seismic events of the main frac (MF) and subsequent four refracs (RF1 to RF4).

Figure 12 Hydraulic fracturing experiment HF3 with progressively increasing flow rate at 19 m depth in borehole F1. Displayed is the flow rate (blue curve) and the interval pressure (red curve) for the mainfrac and the first refrac. The cyclic pressure increase starts with approximately 20 % of the expected formation breakdown pressure based on the previous testing in HF1 and is increased in stepwise cycles (numbers 1 to 5) with a formation breakdown reached at 9.2 MPa (see arrow), which is approximately 30 % lower than during HF1.

Table 3 Results of hydraulic fracturing test HF3 with progressively increasing flow rate at 19 m depth in borehole F1.

Figure 13 Permeability development of the fracturing experiment HF3 with progressively increasing flow rate (main frac MF) (black colored squares and black curve, left axis). For comparison, pressure and seismic events of the different refrac cycles (RF1 to RF4) are also displayed (red curve and red colored dots, right axis).

During the main frac with progressively increased flow rate no fluid recovery was metered, only during the conventional refracs some of the volume was retrieved. The total share is much lower compared to the conventional hydrofracs HF1 and HF2 and is only approximately 13% of the injected volume and mostly from the refracs RF3 and RF4 which are the only stages accompanied by micro-seismic events.

4.4 Conventional hydrofrac test HF4

This test was performed by ISATech and carried out as a conventional test to provide a base line for the upcoming pulse test. The interval is located at 13.65 m depth in fine grained diorite-gabbro. After inflation of the straddle

packers to seal the interval the interval pressure was gradually increased. Flow started when the fracture initiation pressure was reached (Figure 14) and increased until it stabilized. The breakdown pressure was calculated from the distinct event at 10.6 MPa followed by a shut-in (see arrow in Figure 14). The refrac pressure was determined from the first RF and was clearly visible due to the restart of flow and yielded 9.0 MPa (see arrows in Figure 14). Minimum principal stress was estimated from the ISIP after RF1 and resulted in 8.5 MPa. In this test only one seismic event was registered during RF1, but permeability was increased from 0.2 mD after the main frac to 2.7 mD after RF1 and to 3 mD at the end of RF2 (Table 4). During the 3rd RF the generated fracture apparently connected the interval to the borehole behind the packer and the test had to be abandoned due to this leakage. During testing recovery flow (backflow) was not measured due to technical problems.

Figure 14 Conventional hydraulic fracturing experiment HF4 at 13.65 m depth in borehole F1. Displayed is the flow rate (blue curve), the interval pressure (red curve) of the main frac (MF) and subsequent refracs (RF1 and RF2) and the only seismic event during the first refrac (red colored dot), which occurred during reopening of the fracture. Formation breakdown pressure was determined to be 10.6 MPa as indicated by the arrow. Reopening of the fracture can be clearly associated to the restart of flow as indicated by the two arrows. The respective RFP is 9.0 MPa.

Figure 15 Permeability development of the conventional fracturing experiment HF4 main frac (MF) (black colored squares and black curve, left axis). For comparison, pressure and the single seismic event of the two refrac cycles (RF1 and RF2) are also displayed (red curve and red colored dot, right axis).

Table 4 Results of conventional hydraulic fracturing experiment HF4 at 13.65 m depth in borehole F1.

4.5 Pulsed hydraulic fracturing test HF5

The fracturing test HF5 was performed as a dynamic pulse test with progressively increasing flow rate and pressure pulses on top (see schematic in Figure 4). The test was carried out at a borehole depth of 11.3 m in fine grained diorite-gabbro, the same rock type as of test HF4. To obtain the pressure pulses, they were set to initial pressure values of 2, 4, 6 and 8 MPa and a pressure pulse on top, respectively. During the first pressure pulse the pressure increased from 2 to 4 MPa, for the second pulse from 4 to 8.8 MPa and for the third pulse from 6 to 8.6 MPa (Figure 16). The fourth pressure pulse is characterized by a stabilization of pressure without gradual increase indicating the creation of a new fracture during the third pressure pulse. During the third stage a clear pressure drop can be observed and attributed to the breakdown pressure of rock at 9.0 MPa (Figure 17). Thereafter, three RFs were performed and refrac pressure and minimum principal stress are obtained to 8.6 MPa and 7.5 MPa, respectively. During the whole HF5 test no seismic events were recorded, but permeability increased from 2.3 mD after the dynamic pulse stages to 26 mD and 17 mD after the second and third RF (Figure 18 and Table 5). No permeability could be calculated between the pulse stages, because no shut-in was performed between the stages.

Figure 16 Pulsed hydraulic fracturing experiment HF5 at 11.3 m depth in borehole F1. Displayed are the flow rate (blue curve) and the interval pressure (red curve) of the main frac with four increasing flow rate stages and pulses on top.

Figure 17 Third pressure pulse of the pulsed hydraulic fracturing experiment HF5 at 11.3 m depth in borehole F1. Displayed are the flow rate (blue curve), the averaged flow rate (dark blue curve), the interval pressure (red curve) and the averaged pressure (black curve). The visible pressure drop in the averaged pressure curve (indicated by a blue arrow) is attributed to the breakdown of the rock.

Figure 18 Complete sequence of pulsed hydraulic fracturing experiment HF5 including the refrac (reopening) stages (RF1 to RF3) and permeability development. Displayed are the flow rate (blue curve), the interval pressure (red curve) and permeability (black colored squares and line). During the whole HF5 no seismic events were recorded, but permeability increased from 2.3 mD after the dynamic pulse stages to 26 md and 17 md after the second and third refrac, respectively.

Table 5 Results of the pulsed hydraulic fracturing experiment HF5 at 11.3 m depth in borehole F1

No seismic events were recorded during this pulsed hydrofrac HF5 and subsequent refracs. Recovery volumes during the refracs are very low (Table 5) and were measured with flow rates in the order of 0,001 ml/s, which is at the limit of measurement accuracy.

4.6 Conventional hydrofrac test HF6

The HF6 was performed as a conventional hydrofrac and carried out at 4.8 m depth, i.e. close to the tunnel wall, in fine-grained granite. The fracture breakdown pressure was obtained from a distinct pressure drop to 11.3 MPa. Refrac pressure is much lower than for the previous hydrofracs and was estimated to 4.8 MPa. Minimum principal stress was obtained from ISIP to 8.1 MPa. In contrast to the two previous conventional HF tests in fine grained diorite-gabbro this test is accompanied with several seismic events. During the main fracturing 15 events were observed. During the RFs up to 5 events each were registered. Unfortunately the records of the acoustic emissions and the hydraulic tests were not synchronized, therefore the coordination of time was carried out based on the notes of the participants. Based on this coordination most of the acoustic emissions occurred during the fracturing process and at the beginning of shut-in of the interval (Figure 19). Permeability development at the various stages is nearly constant with the highest permeability after the main frac (MF) with 5.6 mD and nearly constant at about 4.3 mD for the refracs (RF1 to RF3).

Figure 19 Conventional hydraulic fracturing experiment HF6 at 4.8 m depth in borehole F1. Displayed is the flow rate (blue curve), the interval pressure (red curve), the seismic events (red dots) of the main frac (MF) and subsequent refracs (RF1 to RF3).

Figure 20 Permeability development of the conventional fracturing experiment HF6 (black colored squares and black curve, left axis). For comparison, pressure and the seismic events are also displayed (red curve and red colored dots, right axis). After the main frac (MF) permeability stabilizes at a nearly constant level for the subsequent refracs (RF1 to RF3).

Table 6 Results of conventional hydraulic fracturing experiment HF6 at 4.8 m depth in borehole F1

The number of acoustic events during hydrofrac HF6 increases with injected volume similar to the results of HF1 and HF2. Total recovery volume is only 2 % of the injected volume and again very low in contrast to the hydrofracs HF1 and HF2.

5 Discussion

Conventional hydraulic fracturing tests and fracturing tests with special protocols were performed in the Äspö Hard Rock Laboratory (HRL) to study the prospects of reducing the number and magnitudes of seismic events and simultaneously enhance the permeability of the fractured intervals. During the fracturing test with progressively increasing flow rate no acoustic events were measured (Figure 21), which is at least an indication of a very low seismicity, which is below the threshold of the monitoring system. Only during the 3rd refrac and the 4th refrac one and 15 events were recorded, respectively. During the conventional treatments carried out in the same rock type (Ävrö Granodiorite) approximately 6 m (HF1) and 3.5 m apart (HF2) several seismic events were recorded during all stages including the Main fracs (Figure 21). Permeability development for the conventional hydrofracs is accompanied with an increase of acoustic events. The highest increase of permeability is attributed to the refracs with the largest number of events, i.e. RF5 at HF1 and RF5 at HF2.

Figure 21 Permeability development (colored squares) and corresponding seismic events (colored diamonds) with the conventional hydraulic fracturing test procedures (HF1 (red) and HF2 (green)) and with the progressively increasing flow rate protocol (HF3 (blue)). The main frac of HF3 consists of 5 cycles with progressively increasing flow rate (details in Figures 11 and 12), where permeability is calculated separately from the pressure decline after each cycle.

The images of the impression packer tests (see Appendix B) show one fracture trace and two adjacent fractures for the conventional HF1 and HF2 respectively. Orientations of the fractures from the impression packer tests are shown in Table B1 (Appendix B and Figure 22). The fracturing test HF3 with increasing flow rate shows a different

behavior with one steeply dipping fracture trace and two nearly parallel fracture traces. This is a clear indication of multiple fracture initiation with different fracture orientation generated during this special protocol with progressively increasing flow rates. The derived acoustic events from the AE hypocenter distribution correlate roughly with the impression packer orientations of HF1 to HF3 and show a clear outward propagation (Figure 22) (Kwiatek et al. 2017; Zang et al. 2017a). The fracture extension obtained from AE analysis is 5.3 m and 6.7 m for HF1 and HF2, respectively; for HF3 the extension is with 2.3 m lower than the previous tests and extension in different direction according to the two generated fractures with one with a higher dip and one with a lower dip (Figure 23).

Figure 22 Orientations of the impression packer tests and the derived acoustic events from the AE hypocenter distribution of tests HF1 to HF3.

Figure 23 Fracture extensions obtained from the AE analysis for the tests HF1 to HF6 with the exception of HF5, which did not show any AE activities. The upper part a) presents the map view, the lower part b) a side view with a direction as indicated by the arrow in part a). The AE activities are color coded for the different tests and outline the fracture extensions of the experiments (modified from Zang et al., 2017a).

The pulsed hydraulic stimulation (HF5) and one conventional hydrofrac (HF4) were carried out in fine-grained diorite-gabbro to provide the comparison of the outcome of both treatments. Regarding the occurrence of seismicity only one event was observed during the conventional treatment, therefore the advantage of a pulsed treatment could not be quantitatively proven due to the lack of enough numbers of events. The development of permeability is similar for both treatments if all refracs are included, whereas the breakdown pressure is lower in the pulse testing. Therefore, the reduced pressure needed to fracture the rock and the lack of any seismic events is a strong indication of the general advantage of a pulsed treatment if the risk of unwanted high seismicity is of concern.

The images of the impression packer tests (Appendix B) show different characteristics for the two tests in fine grained diorite-gabbro. In HF4 four different fracture traces can be distinguished, whereas in HF5 one fracture trace is hardly visible. HF4 is only accompanied with one single acoustic event, HF5 did not show any event. The lack of seismicity may be attributed to a more ductile behavior of the diorite-gabbro with low seismicity compared to the granodiorites of HF1 to HF3 and the granites of HF6. In HF6 four fracture traces could be identified and are in line with orientation and propagation of acoustic events (Zang et al. 2017a).

During the stimulations with the two advanced protocols the permeability increase seems to be lower compared to the conventional fracs and, in particular, the observed increase of permeability during the refracs is more pronounced. But this disadvantage is compensated by the reduced number of seismic events accompanied with these treatments. In contrast to the conventional hydraulic fracturing tests no seismicity was recorded at both advanced protocol tests.

6 Conclusion

The risk of unwanted high seismic events during and after hydraulic stimulation treatments is a major concern in geothermal site developments and can lead to the suspension of the projects due to the loss of acceptance of the authorities and the general public. To address this problem experiments under safe conditions at smaller scales within mines or the laboratory like the hard rock laboratory in Äspö, Sweden, offer the opportunity to perform a larger number of these kinds of hydraulic tests without the risk of any harm or damage to the environment. The results can then be used for a better understanding of the fracturing processes and the accompanied seismic events to redesign the schedule of field experiments accordingly.

The cyclic stimulation scheme with an increase and decrease of the fracturing net pressure seems to lead to a lower seismicity but increases the permeability of the treated rock intervals. In this study the trend of permeability enhancement is lower for the experiments with progressively increased flow rates (HF3 and HF5) compared to the other conventional treatments. However, to confirm this, further experiments are required. In conclusion, to achieve the same permeability increase the hydraulic stimulation treatments will take longer and hence are more costly. Despite these limitations, in field applications with expected high risk of unwanted seismic events, this advanced protocol can be a feasible option to reduce this risk.

7 Acknowledgements

The geothermal project described in this manuscript was financially supported by GFZ German Research Center for Geosciences, Potsdam (75 per cent), KIT Karlsruhe Institute of Technology (15 per cent) and Nova Center for University Studies, Research and Development, Oskarshamn, Sweden (10 per cent). An additional in-kind contribution of SKB for using Äspö Hard Rock Laboratory as test site for geothermal research is greatly acknowledged. The assistance of Felix Becker (MeSy-Solexperts, Bochum) and O. Vanecek and J. Skalova (ISATech, Prague) in performing the hydraulic field tests is greatly appreciated.

8 References

Ask D (2003) Evaluation of measurement-related uncertainties in the analysis of overcoring rock stress data from Äspö HRL, Sweden: a case study. Int J Rock Mech Min Sci 40(7-8) :1173–1187

Ask D (2006a) New developments in the Integrated Stress Determination Method and their application to rock stress data at the Äspö HRL, Sweden. Int J Rock Mech Min Sci 43(1) :107–126

Ask D (2006b) Measurement-related uncertainties in overcoring data at the Äspö HRL, Sweden. Part 2: Biaxial tests of CSIRO HI overcore samples. Int J Rock Mech Min Sci 43(1):127–138

Deon F Regenspurg S Zimmermann G (2013) Geochemical interactions of Al2O3-based proppants with highly saline geothermal brines at simulated in situ temperature conditions. Geothermics 47:53-60.

Economides MJ Nolte KG (2000) Reservoir Stimulation 3rd Edition. Wiley and Sons Ltd. United Kingdom

Häring M Ö Schanz U Ladner F Dyer BC (2008) Characterisation of the Basel 1 enhanced geothermal system. Geothermics 37:469–495

Haimson B Cornet F (2003) ISRM Suggested Methods for rock stress estimation Part 3: hydraulic fracturing (HF) and/or hydraulic testing of pre-existing fractures (HTPF). Int J Rock Mech Min Sci 40(7-8) :1011–1020

Horne RN (1995) Modern Well Test Analysis: A Computer-Aided Approach 2nd ed. Petroway Inc.

Johnson DE Wright TB Tambini M Maroli R Cleary MP (1993) Real-data on-site analysis of hydraulic fracturing generates optimum procedures for job design and execution. SPE 25920

Kiel OM (1977) The Kiel process - Reservoir stimulation by dendritic fracturing. Soc Pet Eng SPE-6984-MS 1-29

Klee G Rummel F (2002) IPR-02-02 Rock stress measurements at the Äspö HRL Hydraulic fracturing in boreholes. Tech Rep SKB

Kwiatek G Bohnhoff M Dresen G Schulze A Schulte T Zimmermann G Huenges E (2010) Microseismicity induced during fluid-injection: A case study from the geothermal site at Groß Schönebeck, North German Basin. Acta Geophysica 58 (6) :995-1020

Kwiatek G Plenkers K Martinez Garzon P Leonhardt M Zang A Dresen G (2017) New insights into fracture process through in-situ acoustic emission monitoring during fatigue hydraulic fracture experiment in Äspö Hard Rock Laboratory. Procedia Engineering 191 :618—622

Legarth B Huenges E Zimmermann G (2005) Hydraulic fracturing in a sedimentary geothermal reservoir: Results and implications. Int J Rock Mech Min Sci 42 :1028–1041

Lopez Comino J, Heimann S, Cesca S, Milkereit C, Dahm T, Zang A (2017a) Automated Full Waveform Detection and Location Algorithm of Acoustic Emissions from Hydraulic Fracturing Experiment. - Procedia Engineering, 191, 697-702

Lopez Comino J, Heimann S, Cesca S, Grigoli F, Milkereit C, Dahm T, Zang A (2017b) Characterization of hydraulic fractures growth during the Äspö Hard Rock Laboratory Experiment (Sweden), Rock Mech Rock Eng 50, 2985–3001

Majer El Baria R Stark M Oates S Bommer J Smith B Asanuma H (2007) Induced seismicity associated with Enhanced Geothermal Systems. Geothermics 36 :185-222

Palisch T Duenckel R Wilson B (2015) New Technology Yields Ultrahigh-Strength Proppant. SPE Production and Operations SPE-168631-PA 76-81.

Patel SM Sondergeld CH Rai CS (2017) Laboratory studies of hydraulic fracturing by cyclic injection. International Journal of Rock Mechanics & Mining Sciences 95:8-15

Reinicke A Blöcher G Zimmermann G Huenges E Dresen G Stanchits S Legarth B A Makurat A (2013) Mechanically induced fracture-face skin: Insights from laboratory testing and modeling approaches. SPE Production & Operations 28(1):26-35

Schubarth S Milton-Tayler D (2004) Investigating how proppant packs change under stress. SPE 90562

Shen B Stephansson O Rinne M (2014) Modelling Rock Fracturing Processes: A Fracture Mechanics Approach Using FRACOD. Springer Science & Business Media, Dordrecht

Tester JW Anderson BJ Batchelor AS Blackwell DD DiPippo R Drake EM Garnish J Livesay B Moore MC Nichols KM Petty S Toksöz MN Veatch Jr RW Baria R Augustine C Murphy E Negraru P Richards M (2006) The Future of Geothermal Energy: Impact of Enhanced Geothermal Systems (EGS) on the United States in the 21st century. Massachusetts Institute of Technology ISBN: 0-615-13438-6

Yoon JS Zimmermann G Zang A (2015) Numerical Investigation on Stress Shadowing in Fluid Injection-Induced Fracture Propagation in Naturally Fractured Geothermal Reservoirs. Rock Mech Rock Eng 48 :1439-1454

Yoon JS Zimmermann G Zang A (2015) Discrete element of cyclic rate fluid injection at multiple locations in naturally fractured reservoirs. Int J Rock Mech & Min Sci 74:15-23

Yoon JS Zimmermann G Zang A Stephansson O (2015) Discrete element modeling of fluid injection-induced seismicity and activation of nearby fault. Can Geotech J 52 :1457-1465

Zang A Stanchits S Dresen G (2002) Acoustic emission controlled triaxial rock fracture and friction tests. In: Dyskin AV Hu X Sahouryeh E (eds), Structural Integrity and Fracture, Swets & Zeitlinger, pp 289-294

Zang A Wagner FC Stanchits S Janssen C Dresen G (2000) Fracture process zone in granite. J geophys Res 105(B10) 23651-23661

Zang A Yoon J S Stephansson O Heidbach O (2013) Fatigue hydraulic fracturing by cyclic reservoir treatment enhances permeability and reduces induced seismicity. Geophysical Journal International 195(2):1282-1287

Zang A Stephansson O (2010) Stress field of the Earth's crust. Springer Science & Business Media

Zang A Stephansson O Stenberg L Plenkers K Specht S Milkereit C Schill E Kwiatek G Dresen G Zimmermann G Dahm T Weber M (2017a) Hydraulic fracture monitoring in hard rock at 410 m depth with an advanced fluid-injection protocol and extensive sensor array. Geophysical Journal International 208(2) :790-813

Zang A Stephansson O Zimmermann G (2017b) Keynote: Fatigue Hydraulic Fracturing. Procedia Engineering 191:1126-1134

Zang A Zimmermann G Hofmann H Stephansson O Min KB Kim KY (2018) How to Reduce Fluid-Injection-Induced Seismicity. Rock Mech Rock Eng https://doi.org/10.1007/s00603-018-1467-4
Zhuang L Kim KY Jung SG Diaz MB Park S Zang A Stephansson O Zimmermann G Yoon JS (2016) Laboratory study on cyclic hydraulic fracturing of Pocheon granite in Korea. Abstracts 50th US Rock Mechanics/Geomechanics Symposiumum held in Houston Texas USA 26-29 June 2016 16-163

Zhuang L Kim KY Jung SG Nam YJ Min KB Park S Zang A Stephansson O Zimmermann G Yoon JS (2017) Laboratory evaluation of induced seismicity reduction and permeability enhancement effects of cyclic hydraulic fracturing. In Proceedings 51st US Rock Mechanics/Geomechanics Symposium held in San Francisco, California, USA, 25-28 June 2017 17-757

Zimmermann G Moeck I Blöcher G (2010) Cyclic waterfrac stimulation to develop an Enhanced Geothermal System (EGS) – Conceptual design and experimental results. Geothermics 39 :59-69

Zimmermann G Reinicke A (2010) Hydraulic stimulation of a deep sandstone reservoir to develop an Enhanced Geothermal System: Laboratory and field experiments. Geothermics 39:70-77

Appendix A

Permeability is calculated by decline curve analysis taking into account the superposition principle and assuming infinite acting radial flow:

$$k = \frac{q\ \mu}{4\ \pi\ h\ \Delta p}\ ln(\frac{t_0 + \Delta t}{\Delta t})$$

with h = interval length ; q = flow rate ; μ = dynamic viscosity of fluid ; t_0 = injection time ; Δt = shut-in time ; ln = natural logarithm.

Appendix B

Figures B1 to B6 show the images of fracture traces obtained from impression packer tests for all hydraulic fracturing tests performed in the Äspö Hard Rock Laboratory. The circumference of the packer is about 310 mm, the length of the interval is approximately 1m. Table B1 summerizes the obtained orientations of the fracture traces from the impression packer tests. The corresponding fracture locations in the borehole F1 for HF1 to HF6 are shown in Figure B7.

Figure B1 Impression packer test image at 25 m depth of hydraulic fracturing test HF1

Figure B2 Impression packer test image at 22.5 m depth of hydraulic fracturing test HF2

Figure B3 Impression packer test image at 19 m depth of hydraulic fracturing test HF3

Figure B4 Impression packer test image at 13.65 m depth of hydraulic fracturing test HF4

Figure B5 Impression packer test image at 11.3 m depth of hydraulic fracturing test HF5

Figure B6 Impression packer test image at 4.8 m depth of hydraulic fracturing test HF6

Figure B7 Fracture locations for HF1 to HF6 from Table B1. The orientation of the lines corresponds to the azimuth of the fractures (strike direction), the dip direction is indicated by the adjacent arrow with the dip angle given in degrees. The stress tensor from Ask (2006b) closest to the study site from overcoring solutions ($S1$ = 22.6 MPa, $S2$ = 9.5 MPa, $S3$ = 8.1 MPa) is shown for comparison. Stresses are viewed from above and are projected onto the horizontal plane. The length of each vector is proportional to the corresponding stress magnitude. The spanned angle at the vector tips describe the dip of the stress vector.

Table B1 Orientations of fractures from impression packer tests (θ: fracture strike direction (North over East), β: dip direction (North over East), α: dip (with respect to horizontal))

Stage	t_0 s	Δt s	k 10^{-15} m², mD	Events number	V_{inj} liter	V_{re} liter	q_{mean} liter/min
Main frac	47,2	609,8	0,57	0	0,770	0,5	0,98
RF1	123,8	644,8	0,62	3	2,67	1,5	1,29
RF2	166	642,8	1,06	10	4,41	1,7	1,59
RF3	127,2	621	1,6	12	5,15	1,9	2,43
RF4	61	721,6	1,4	4	4,62	2,3	4,55
RF5	118,4	367	7,1	20	9,24	5,5	4,68
Sum					26,86	13,4	

Table 1 Results of the first conventional hydraulic fracturing experiment HF1 at 25 m depth in borehole F1

Stage	t_0 s	Δt s	k 10^{-15} m², mD	Events number	V_{inj} liter	V_{re} liter	q_{mean} liter/min
Main frac	105,2	312,6	1,32	8	3,8	1,1	1,7
RF1	181,2	308	3,63	6	5	1,9	1,7
RF2	28,6	146,4	3,37	0	1,2	0,6	2,5
RF3	122,4	308	2,68	17	5,5	2,3	2,5
RF4	60,2	332,8	2,97	21	4,8	2,3	4,8
RF5	118	321,4	4,78	50	9,4	3,9	4,8
Sum					29,7	12,1	

Table 2 Results of the second conventional hydraulic fracturing experiment HF2 at 22.5 m depth in borehole F1

Stage	t_0 s	Δt s	k 10^{-15} m², mD	Events number	V_{inj} liter	V_{re} liter	q_{mean} liter/min
Main frac1	6,8	130,2	0,211	0	0,11	0	0,94
Main frac2	7,4	124,8	0,181	0	0,12	0	0,95
Main frac3	9	126,8	0,146	0	0,14	0	0,93
Main frac4	14,2	121,4	0,464	0	0,14	0	0,61
Main frac5	16	128,4	0,429	0	0,13	0	0,47
RF1	124	304,8	0,76	0	3,3	0,3	1,6
RF2	123,2	312,6	1,23	0	5,2	0,3	2,5
RF3	62	303,8	1,08	1	5,6	0,8	5,3
RF4	119,4	309	1,97	15	10,5	1,8	5,3
Sum					25,23	3,2	

Table 3 Results of hydraulic fracturing test HF3 with progressively increasing flow rate at 19 m depth in borehole F1.

Stage	t_0 s	Δt s	k 10^{-15} m², mD	Events number	V_{inj} liter	V_{re} liter	q_{mean} liter/min
Main frac	33,79	400,0	0,22	0	0,27		0,48
RF1	203,19	311,8	2,7	1	1,80		0,53
RF2	206,39	219,5	3	0	2,09		0,61
Sum					4,16		

Table 4 Results of conventional hydraulic fracturing experiment HF4 at 13.65 m depth in borehole F1.

Stage	t_0 s	Δt s	k 10^{-15} m, mD	Events number	V_{inj} liter	V_{re} liter	q_{mean} liter/min
Main frac1	61,6			0	0,18		0,18
Mainfrac2	60,0			0	0,37		0,37
Main frac3	60,2			0	0,48		0,48
Main frac4	64,2	316,2	2,3	0	0,75		0,70
RF1	186,2	305,3	10,5	0	4,27	0,09	1,38
RF2	55,2	308,4	26,4	0	6,47	0,09	7,04
RF3	38,2	311,5	17,2	0	3,84		6,04
Sum					16,37	0,18	

Table 5 Results of the pulsed hydraulic fracturing experiment HF5 at 11.3 m depth in borehole F1

	t_0 s	Δt s	k 10^{-15} m², mD	Events number	V_{inj} liter	V_{re} liter	q_{mean} liter/min
mainfrac	107,0	300,7	5,6	15	8,72	0,14	4,89
RF1	46,2	311,1	4,4	5	5,11	0,14	6,64
RF2	47,4	313,5	4,2	5	5,09	0,14	6,45
RF3	44,6	302,3	4,3	3	5,18	0,10	6,97
Sum					24,1	0,52	

Table 6 Results of conventional hydraulic fracturing experiment HF6 at 4.8 m depth in borehole F1

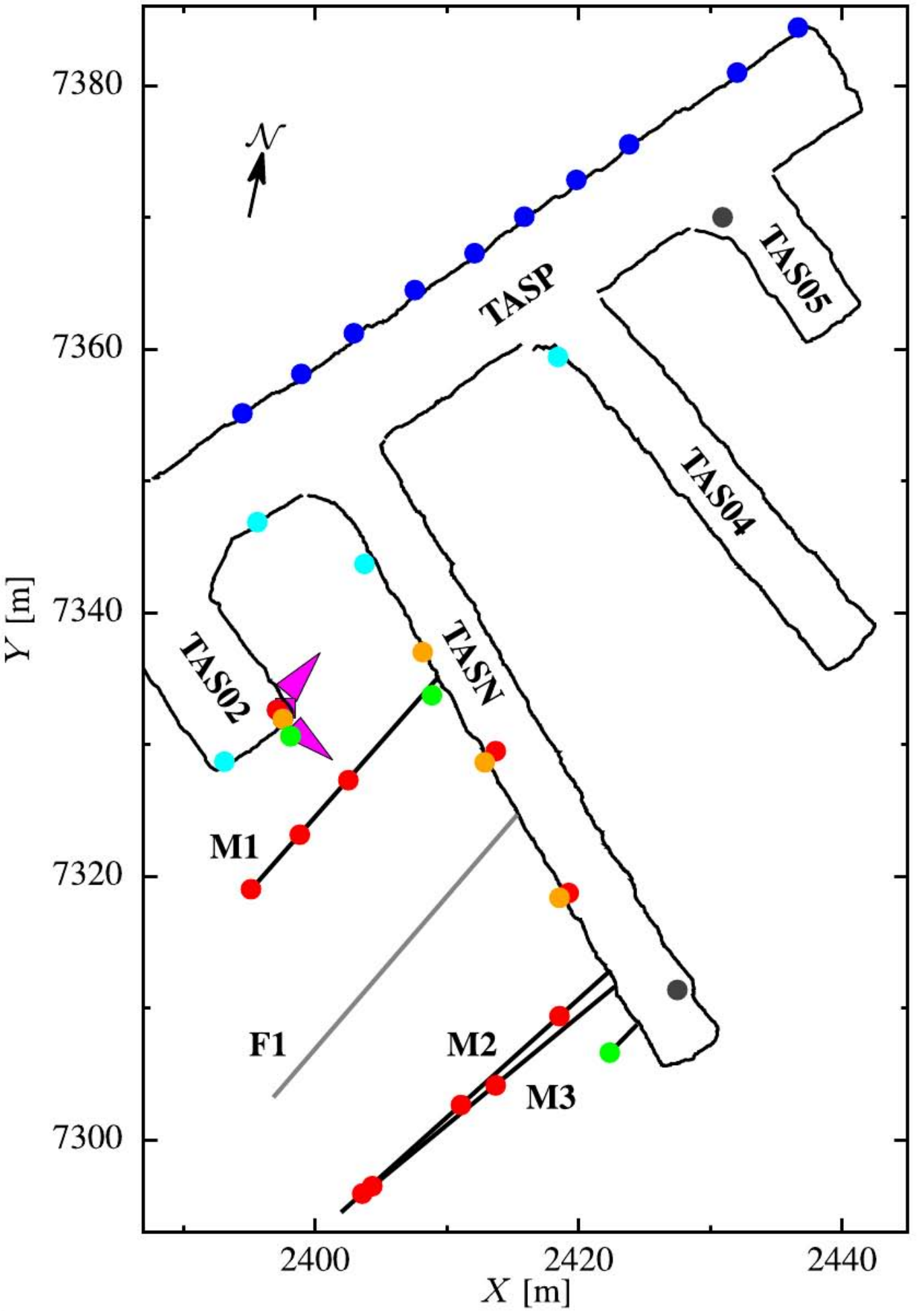
7380
7360
7340
7320
7300
Y [m]
2400
2420
2440
X [m]
N
TASP
TAS05
TAS04
TASN
TAS02
M1
F1
M2
M3

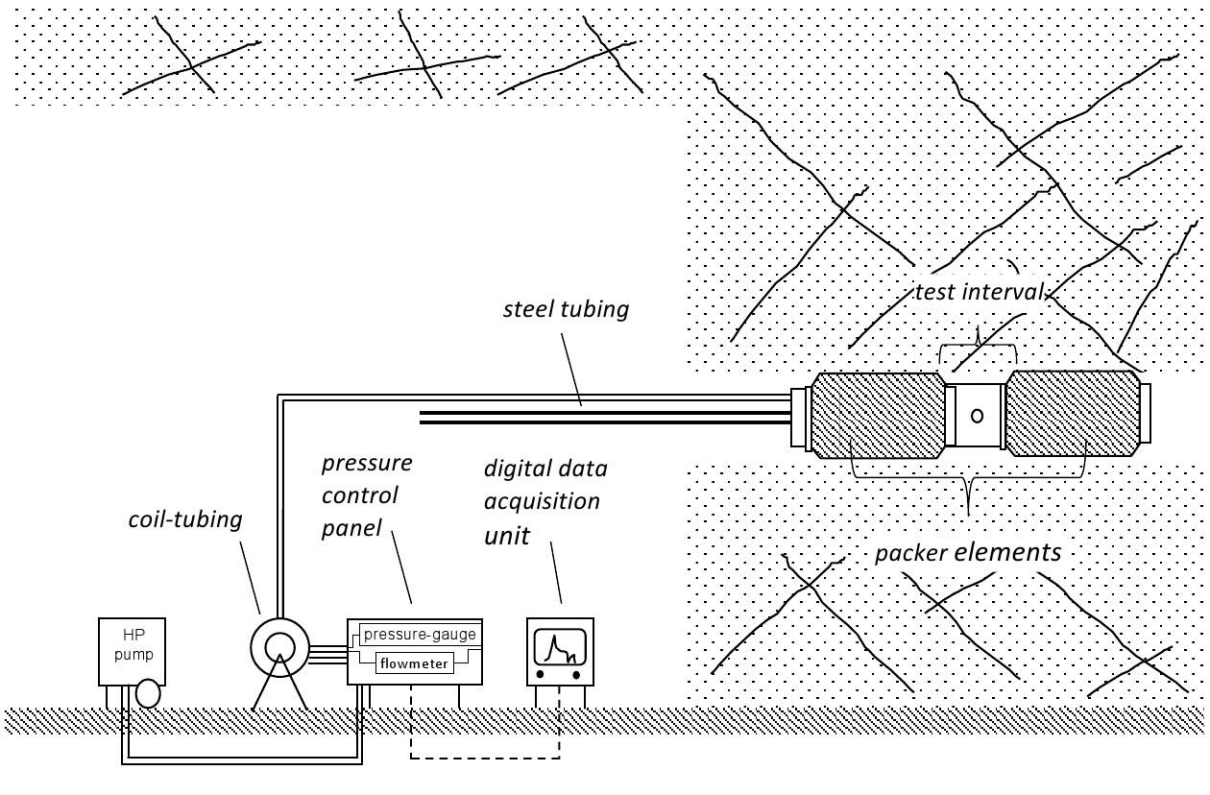
steel tubing
test interval
pressure
control
panel
digital data
acquisition
unit
coil-tubing
packer elements
HP
pump
pressure-gauge
flowmeter


120m
21m
22m
U-224
23m
24m
25m

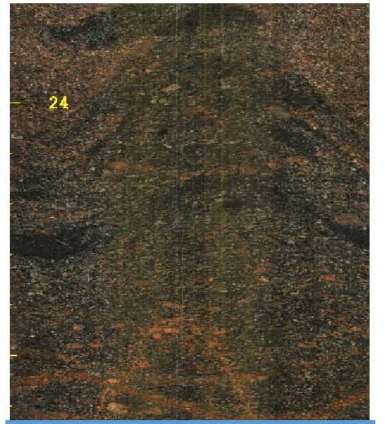
24


25

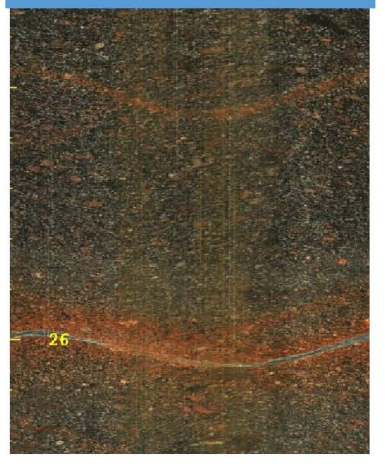
26

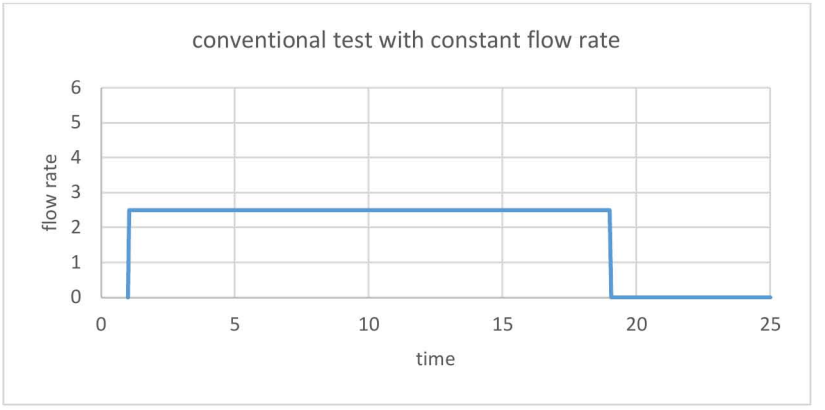
conventional test with constant flow rate
flow rate
time
0
1
2
3
4
5
6
0
5
10
15
20
25

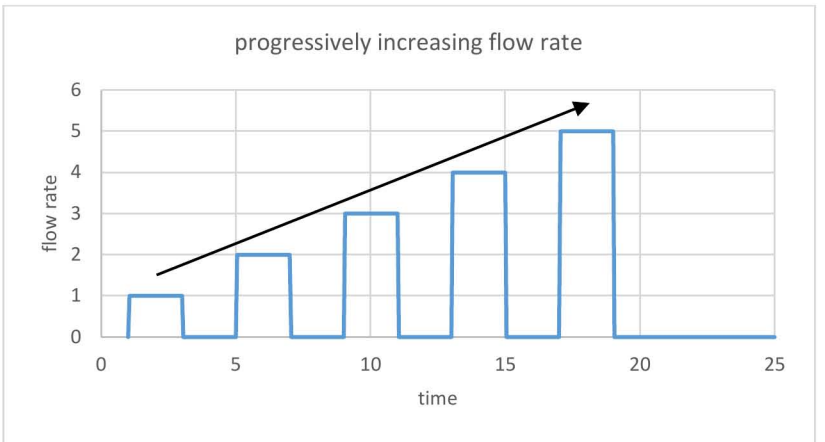
progressively increasing flow rate
flow rate
time
0
1
2
3
4
5
6
0
5
10
15
20
25

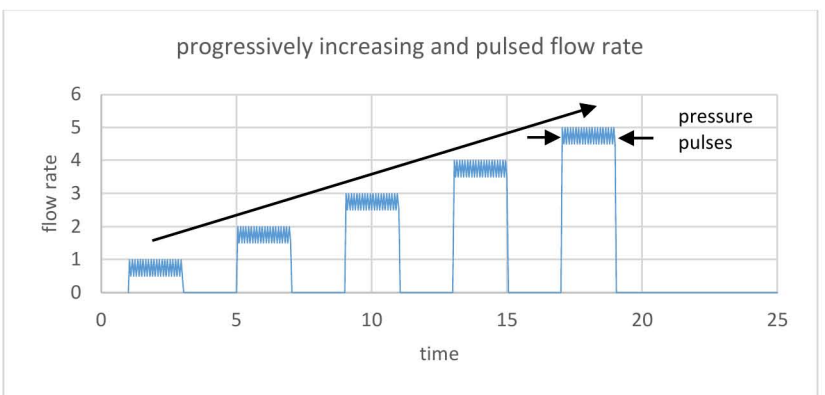
progressively increasing and pulsed flow rate
pressure
pulses
flow rate
time
0
1
2
3
4
5
6
0
5
10
15
20
25

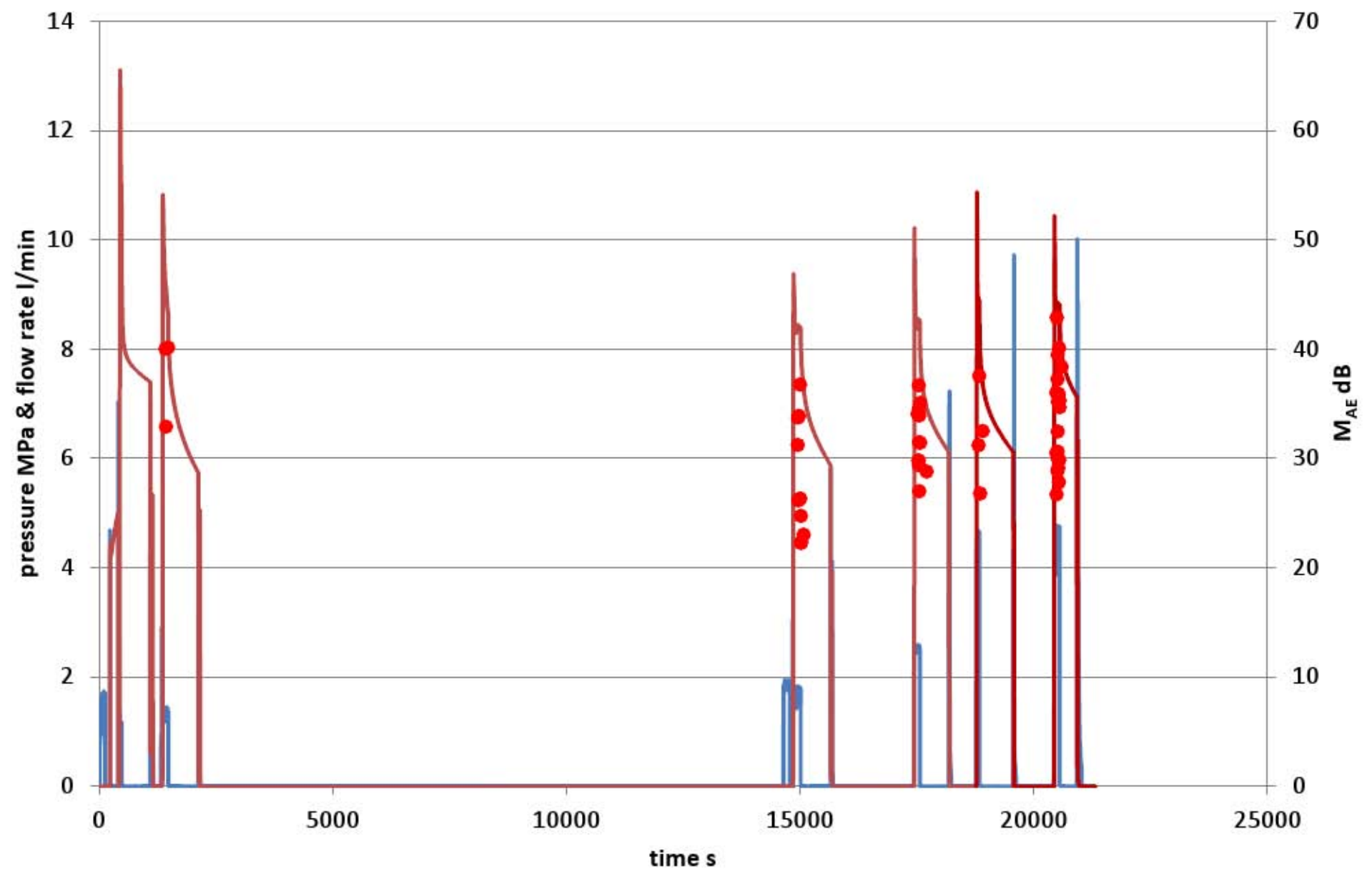
14
12
10
8
6
4
2
0
pressure MPa & flow rate l/min
70
60
50
40
30
20
10
0
M_{AE} dB
0
5000
10000
15000
20000
25000
time s

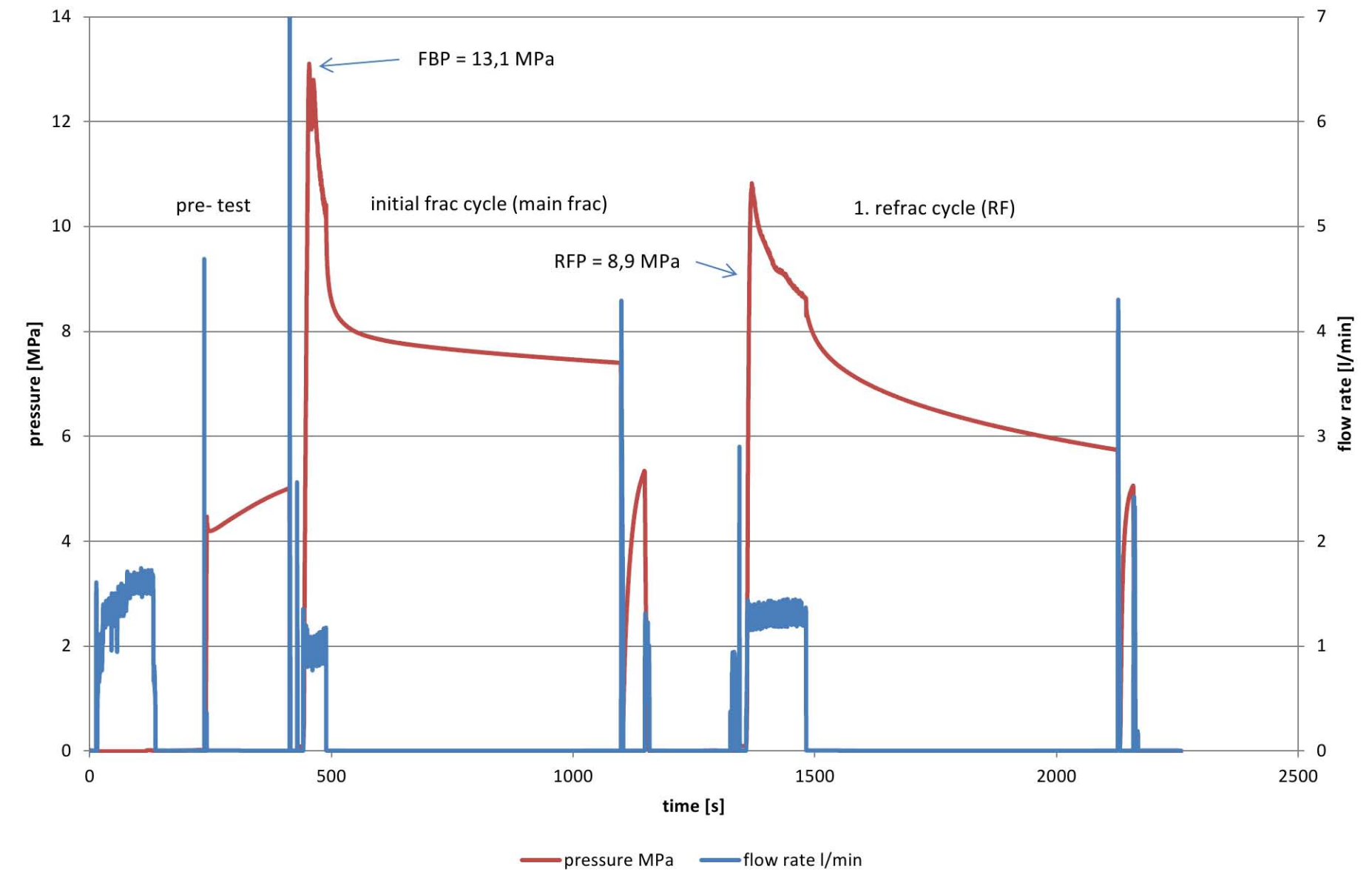
FBP = 13,1 MPa
pre- test
initial frac cycle (main frac)
1. refrac cycle (RF)
RFP = 8,9 MPa
pressure [MPa]
flow rate [l/min]
time [s]
0
500
1000
1500
2000
2500
0
2
4
6
8
10
12
14
0
1
2
3
4
5
6
7
pressure MPa
flow rate l/min

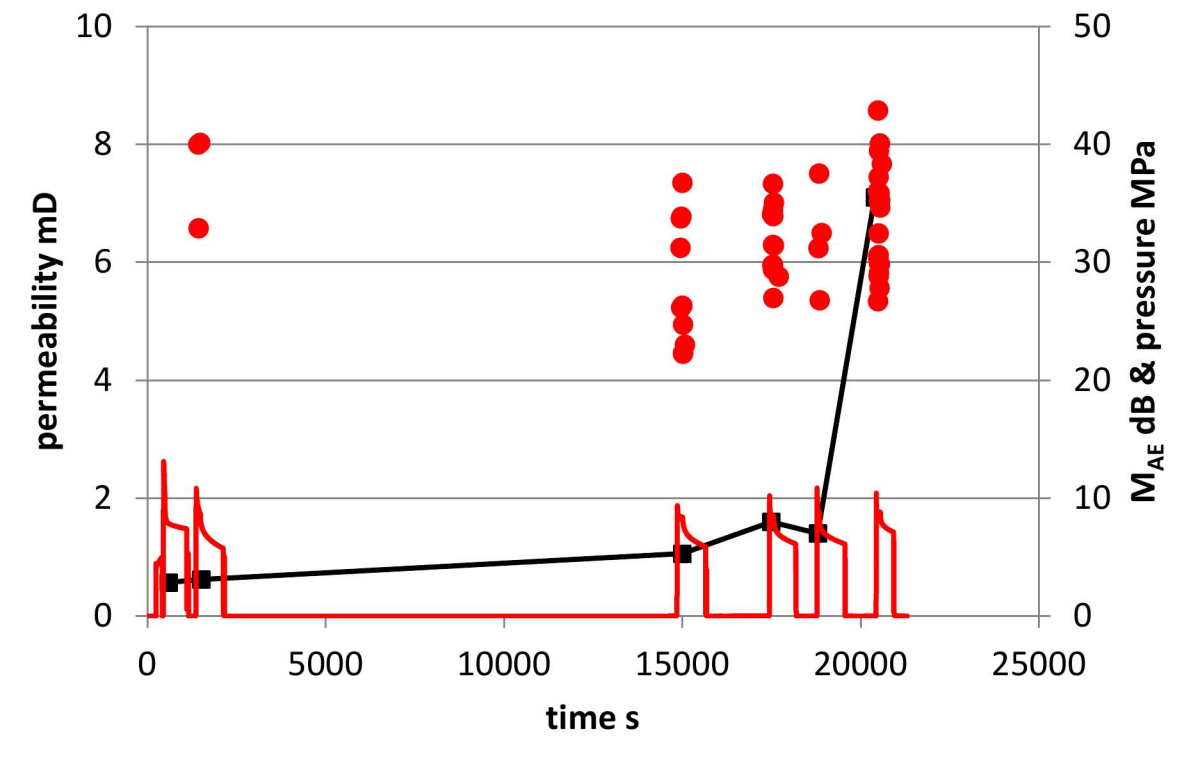
10
8
6
4
2
0
permeability mD
50
40
30
20
10
0
M_{AE} dB & pressure MPa
0
5000
10000
15000
20000
25000
time s

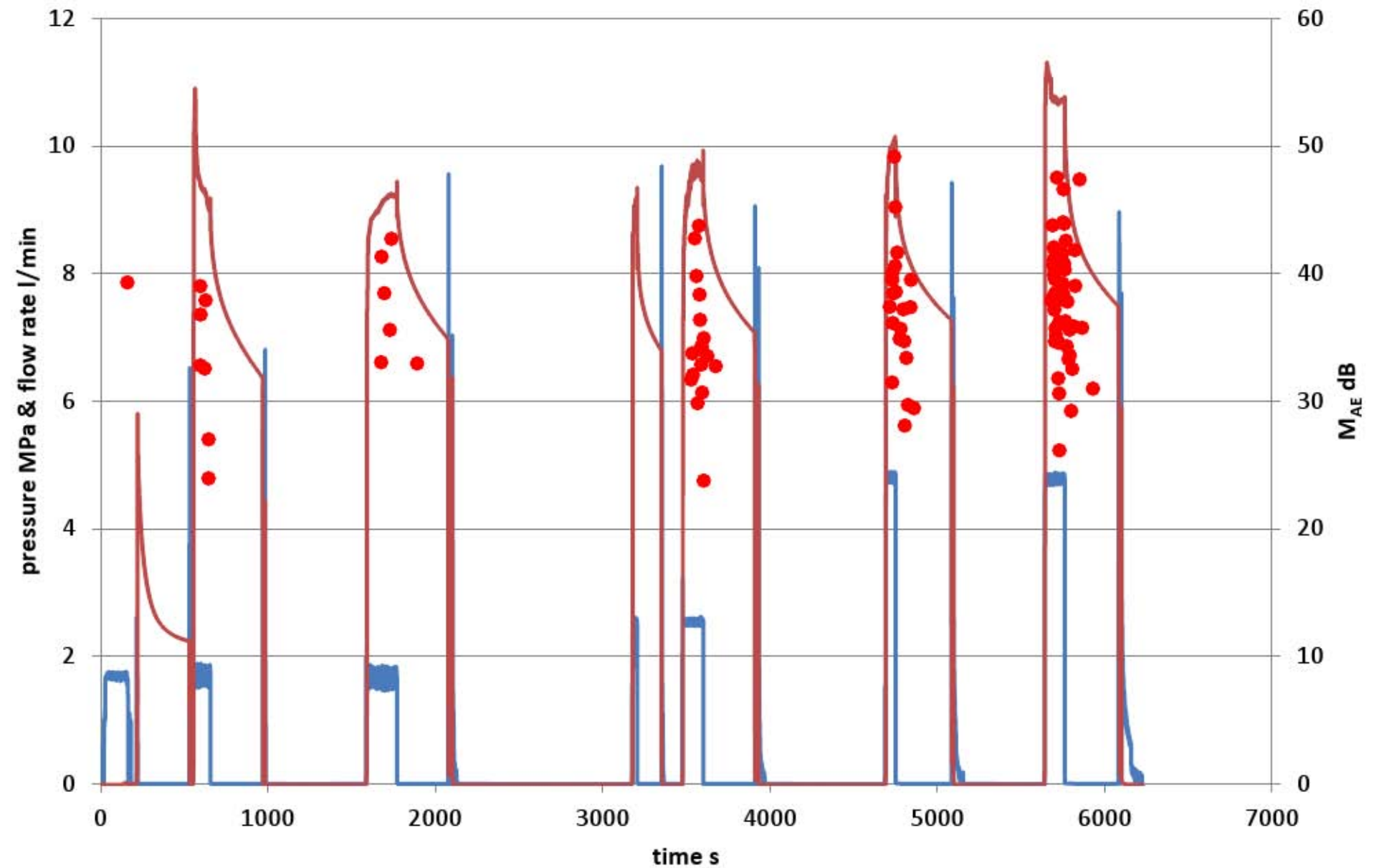
pressure MPa & flow rate l/min
M_{AE} dB
time s
0
2
4
6
8
10
12
0
10
20
30
40
50
60
0
1000
2000
3000
4000
5000
6000
7000

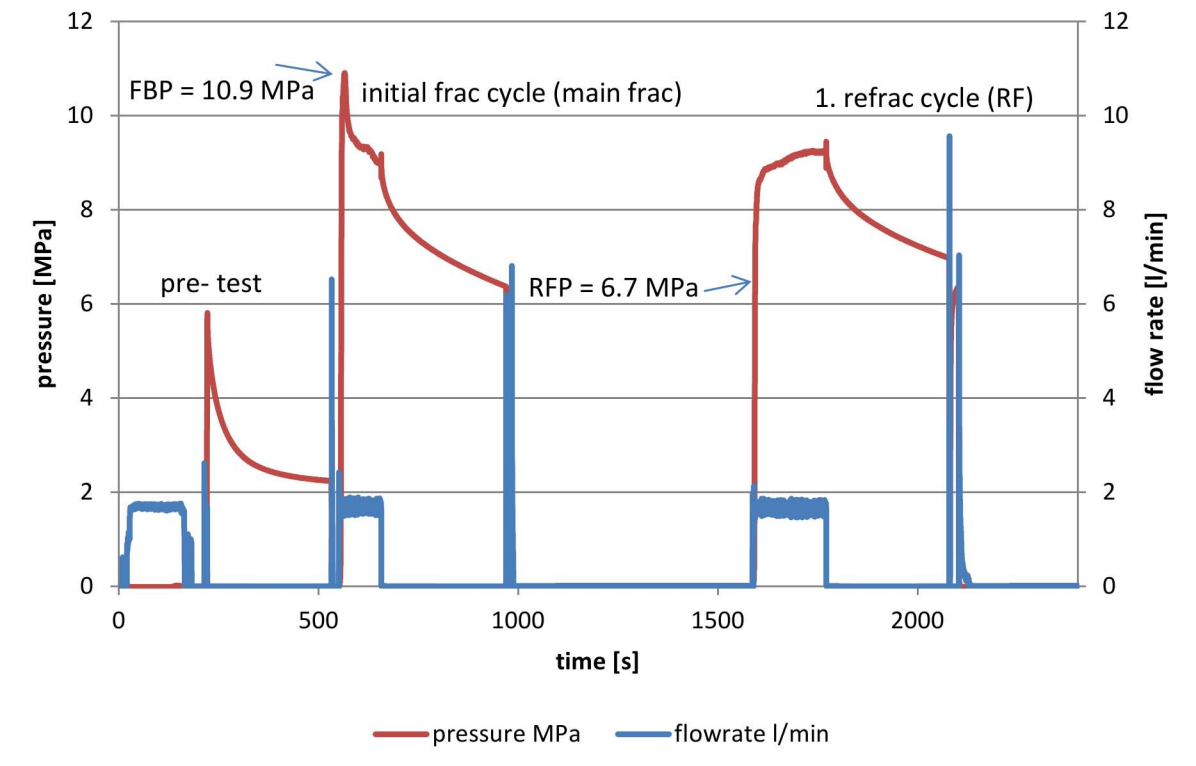
FBP = 10.9 MPa
initial frac cycle (main frac)
1. refrac cycle (RF)
pre- test
RFP = 6.7 MPa
pressure [MPa]
flow rate [l/min]
time [s]
0
500
1000
1500
2000
2
4
6
8
10
12
pressure MPa
flowrate l/min

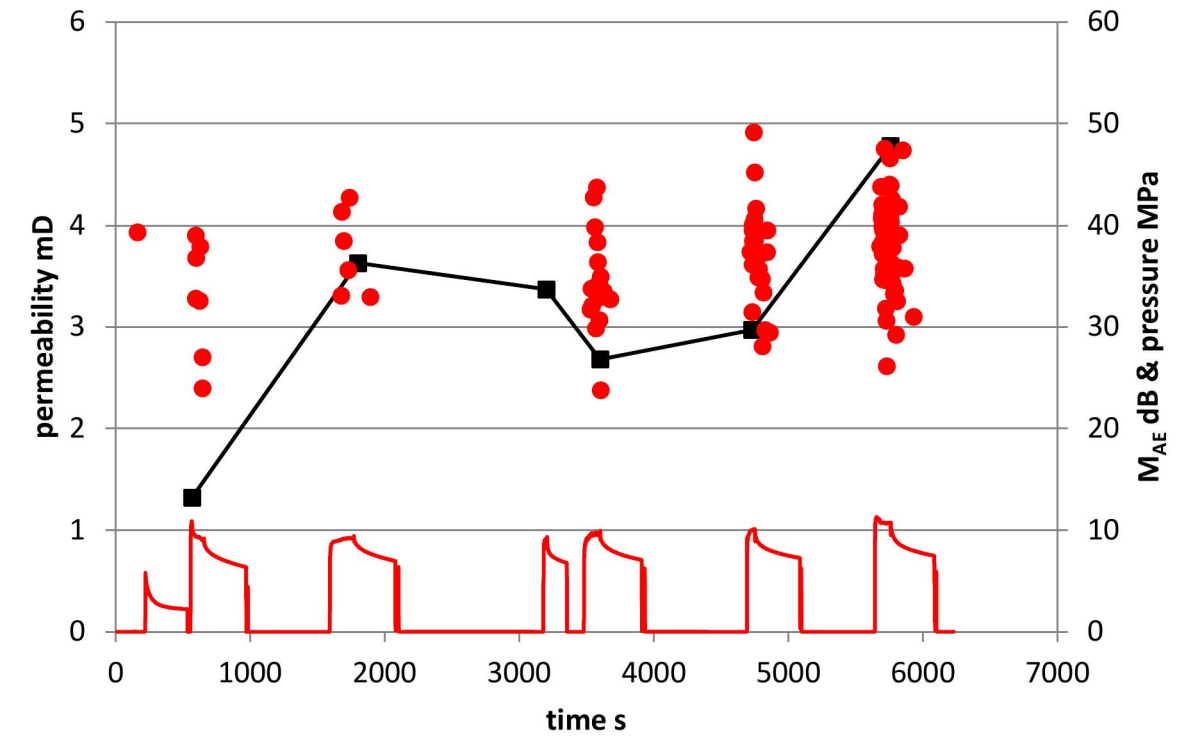
permeability mD
M_{AE} dB & pressure MPa
time s
0
1
2
3
4
5
6
10
20
30
40
50
60
1000
2000
3000
4000
5000
6000
7000

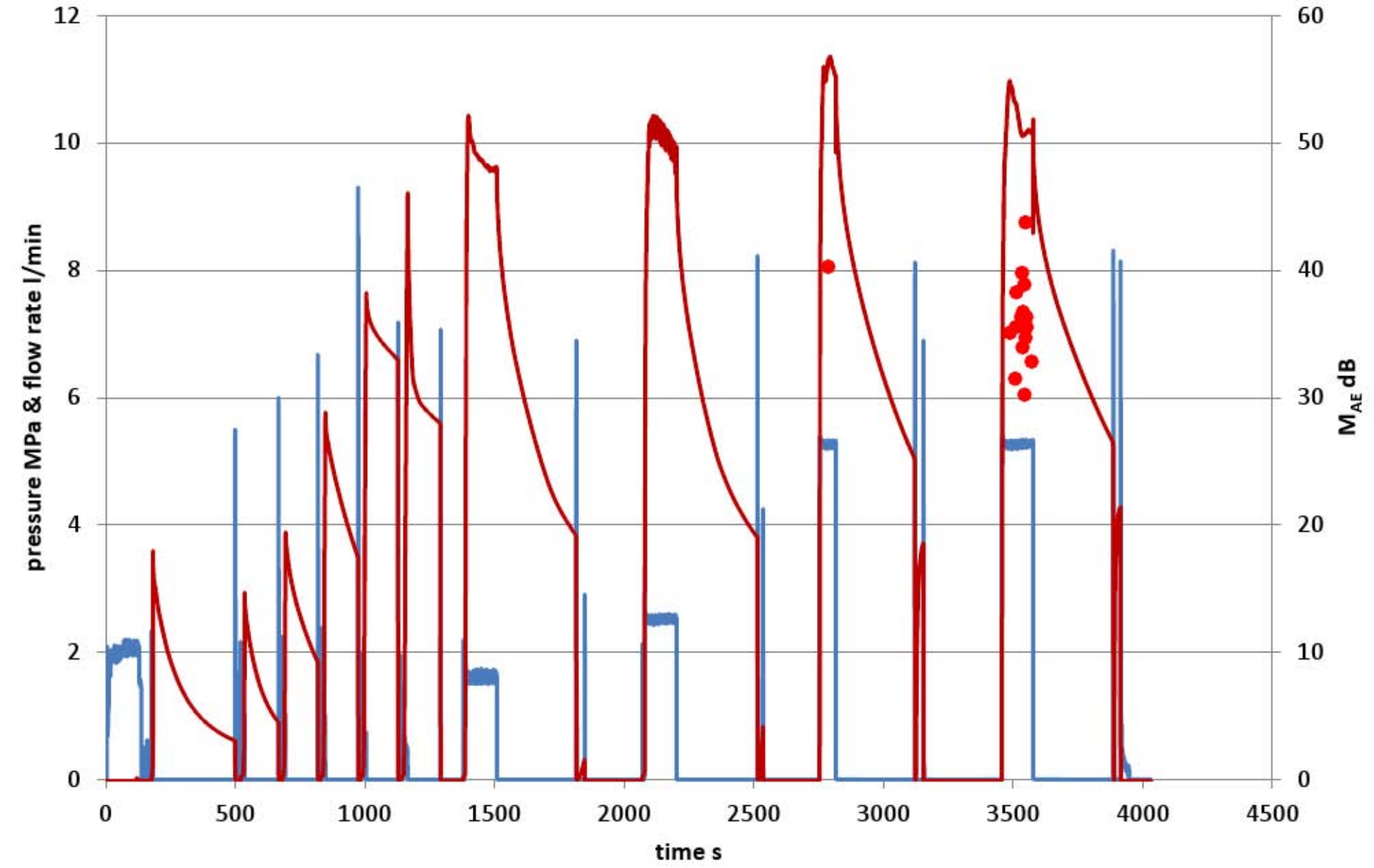
pressure MPa & flow rate l/min
M_{AE} dB
time s
0
2
4
6
8
10
12
0
10
20
30
40
50
60
0
500
1000
1500
2000
2500
3000
3500
4000
4500

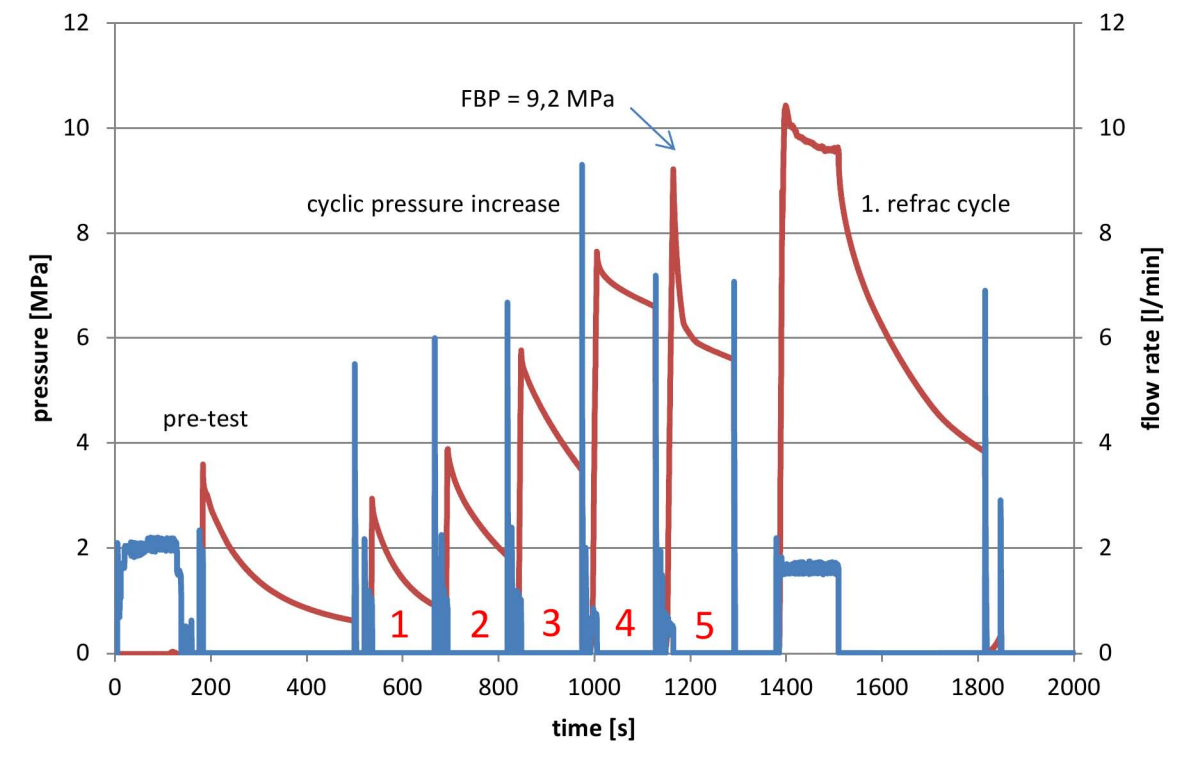
FBP = 9,2 MPa
cyclic pressure increase
1. refrac cycle
pre-test
1
2
3
4
5
pressure [MPa]
flow rate [l/min]
time [s]
0
2
4
6
8
10
12
0
200
400
600
800
1000
1200
1400
1600
1800
2000

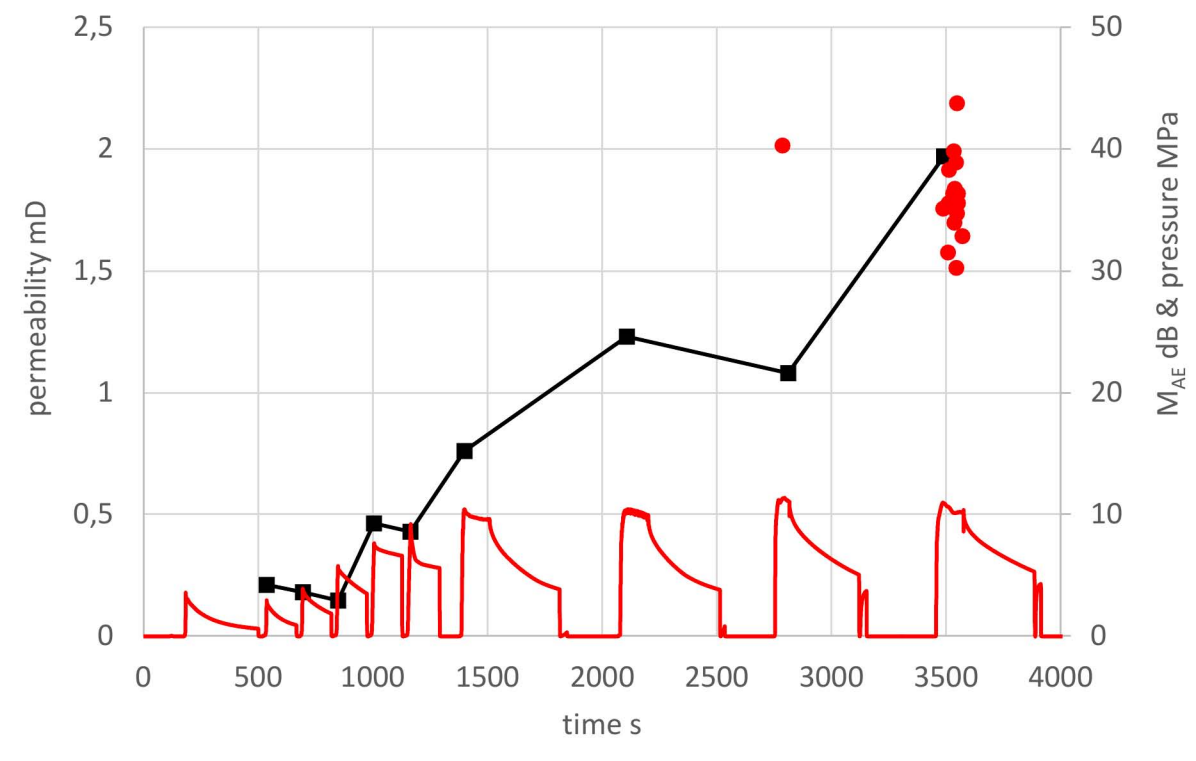
2,5
2
1,5
1
0,5
0
permeability mD
50
40
30
20
10
0
M_{AE} dB & pressure MPa
0
500
1000
1500
2000
2500
3000
3500
4000
time s

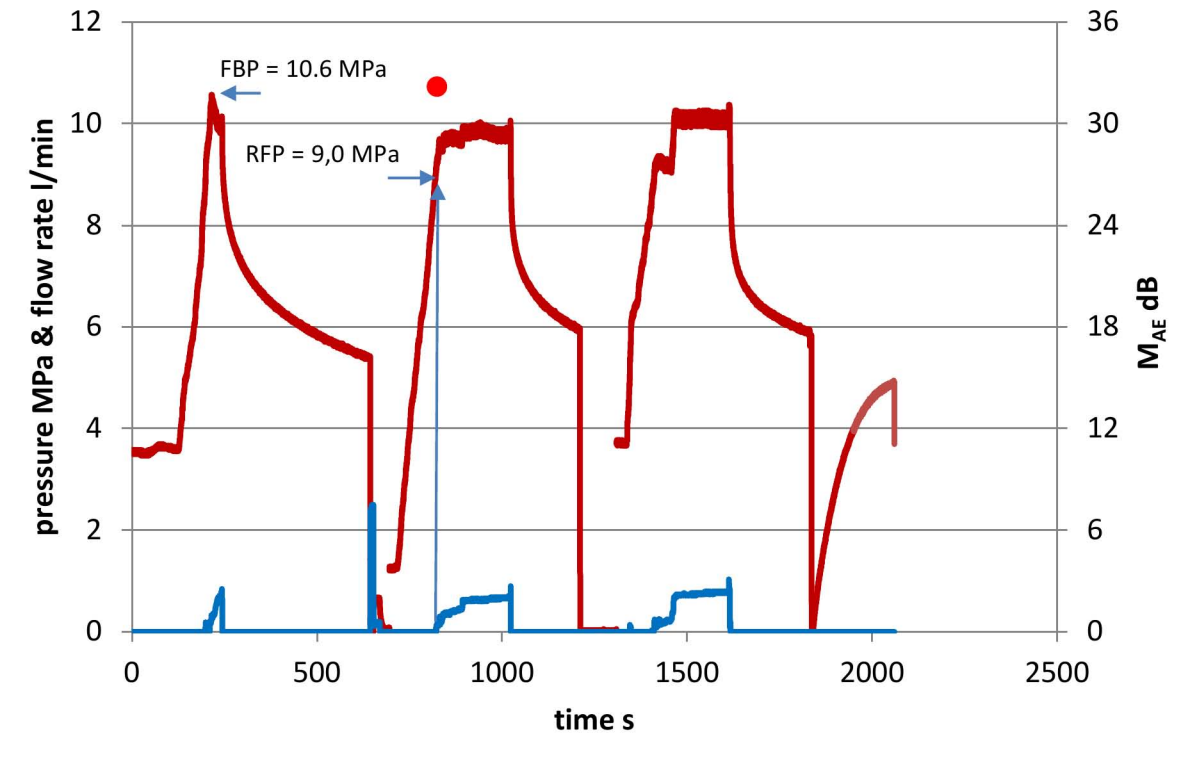
FBP = 10.6 MPa
RFP = 9,0 MPa
pressure MPa & flow rate l/min
M_{AE} dB
time s
0
2
4
6
8
10
12
0
6
12
18
24
30
36
0
500
1000
1500
2000
2500

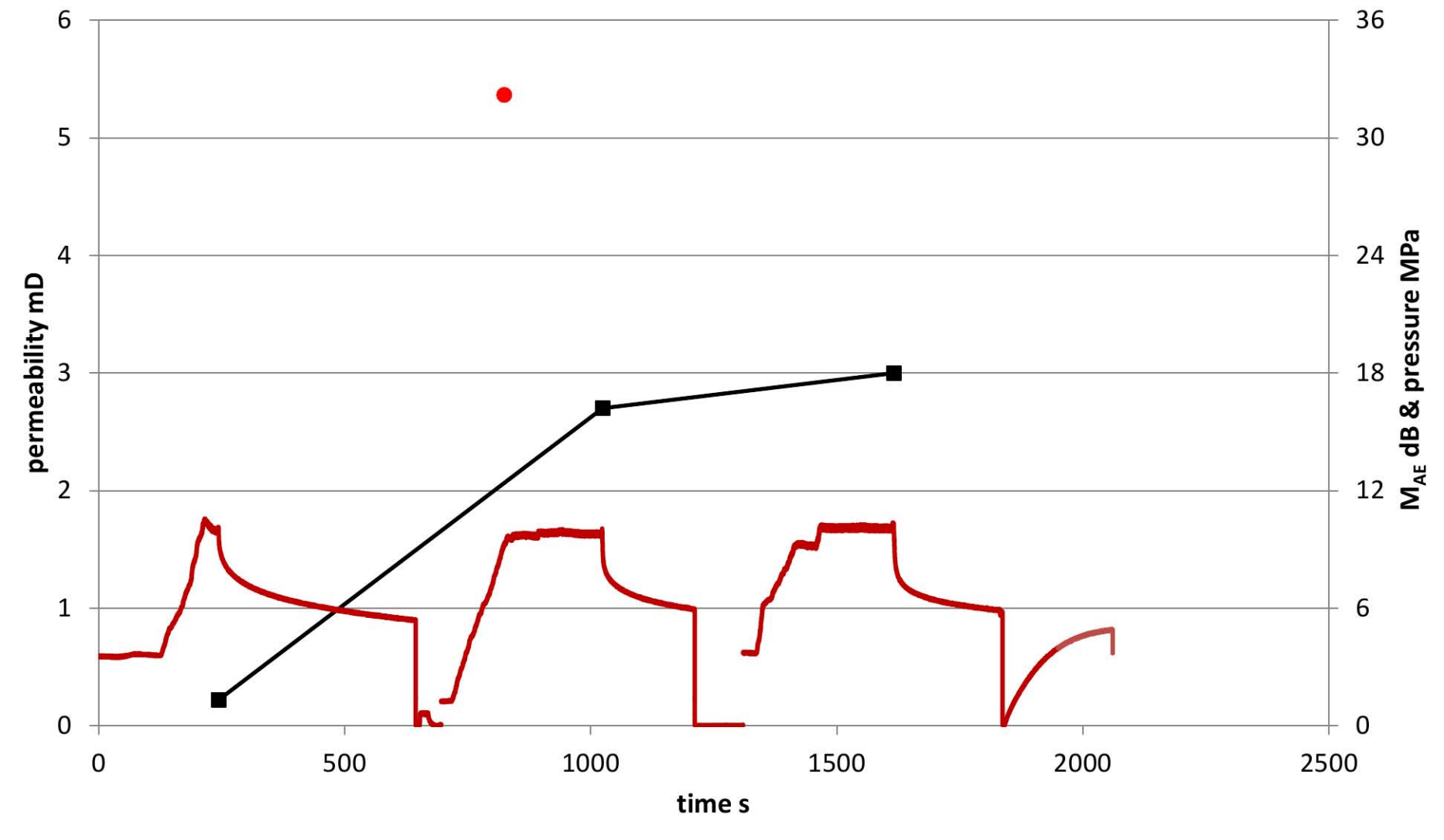
permeability mD
M_{AE} dB & pressure MPa
time s
0
1
2
3
4
5
6
0
6
12
18
24
30
36
0
500
1000
1500
2000
2500

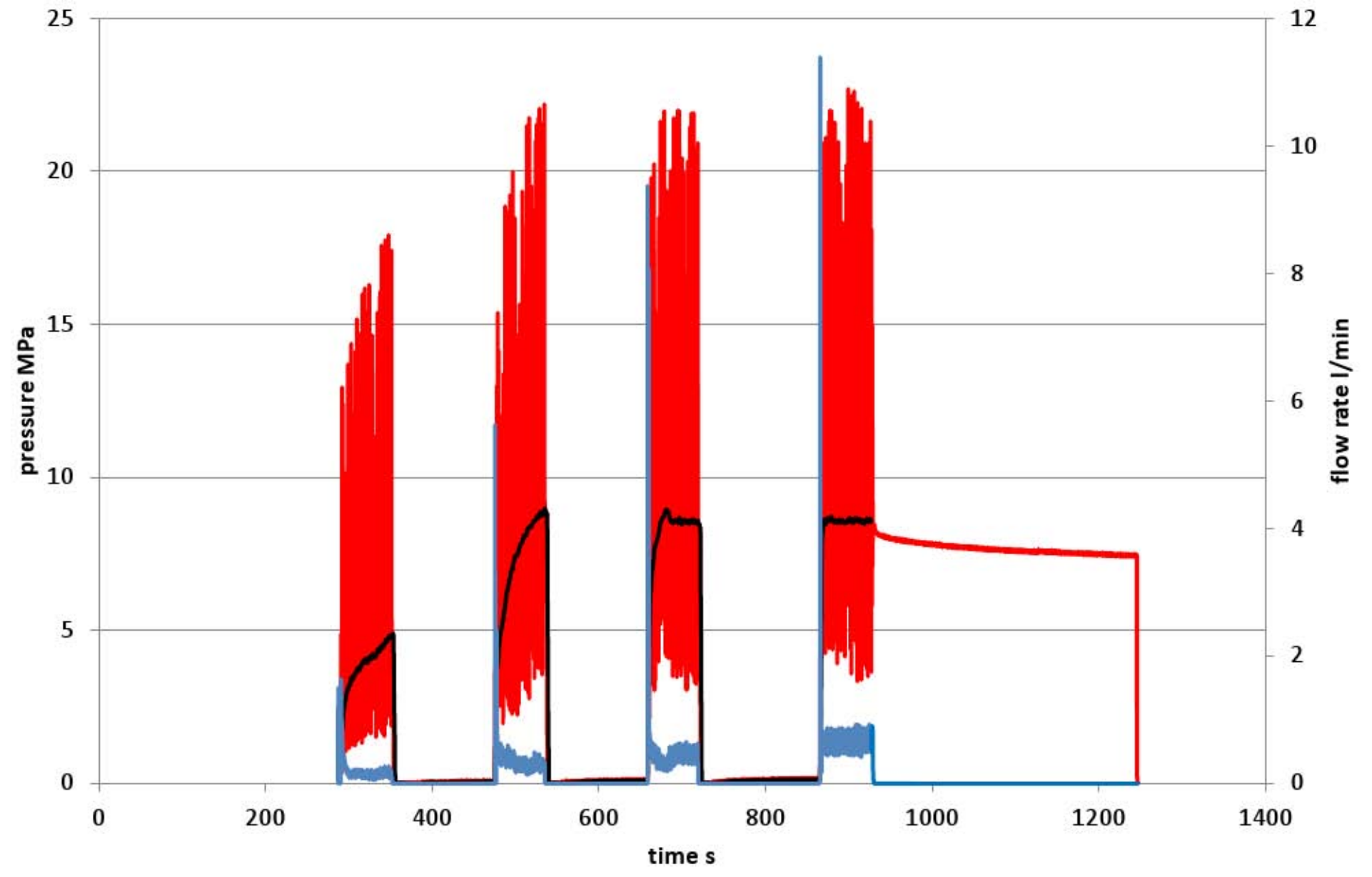
25
20
15
10
5
0
pressure MPa
12
10
8
6
4
2
0
flow rate l/min
0
200
400
600
800
1000
1200
1400
time s

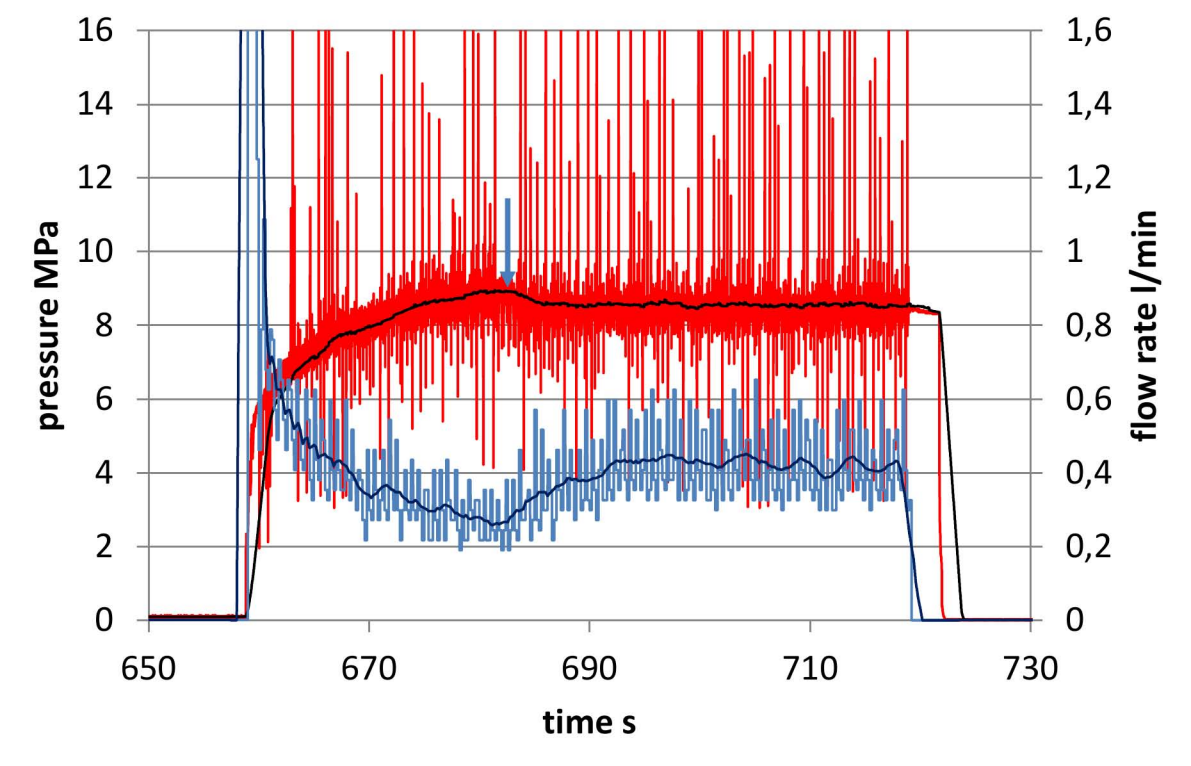
16
14
12
10
8
6
4
2
0
pressure MPa
1,6
1,4
1,2
1
0,8
0,6
0,4
0,2
0
flow rate l/min
650
670
690
710
730
time s

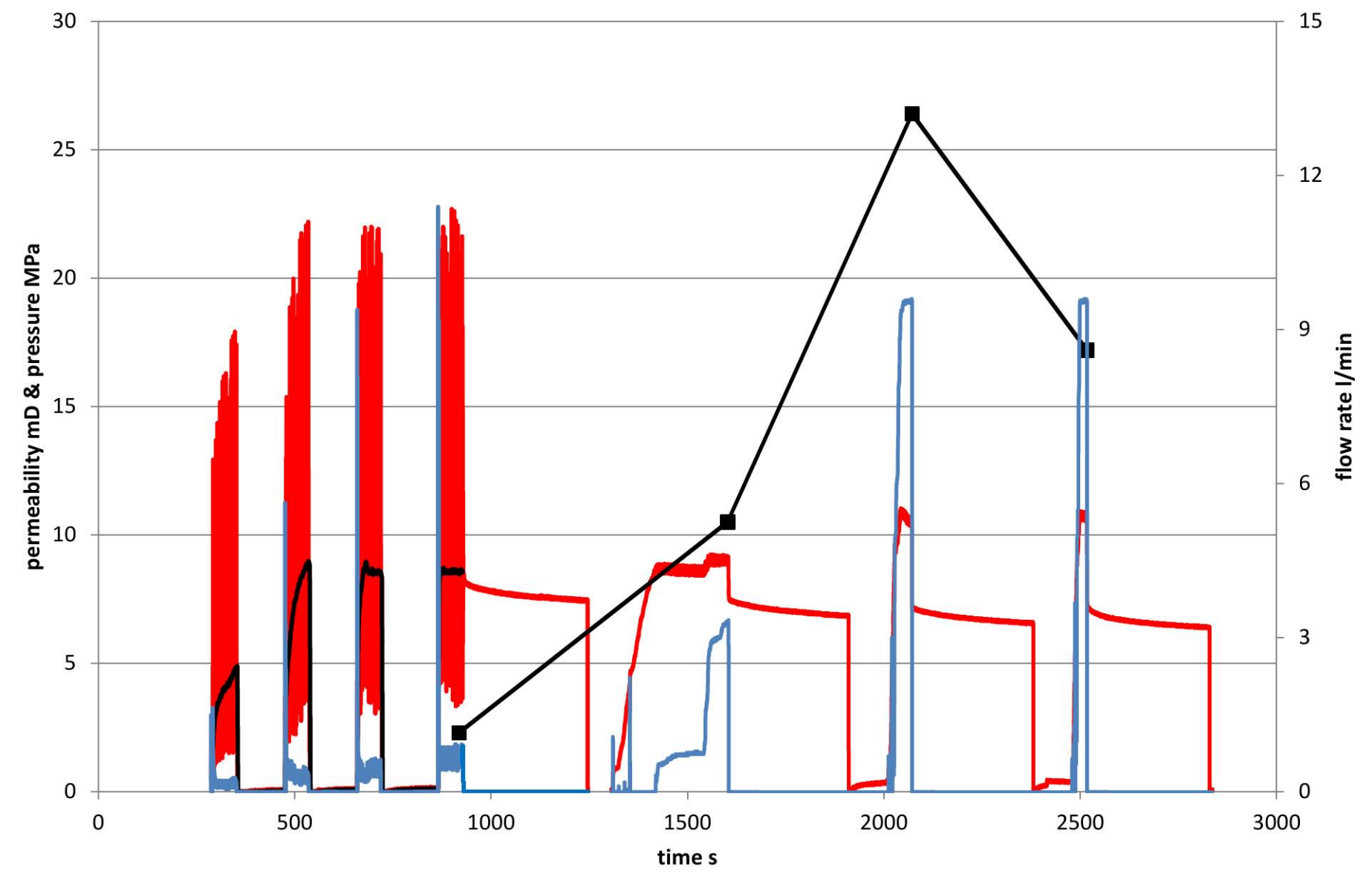
permeability mD & pressure MPa
flow rate l/min
time s
0
5
10
15
20
25
30
0
3
6
9
12
15
0
500
1000
1500
2000
2500
3000

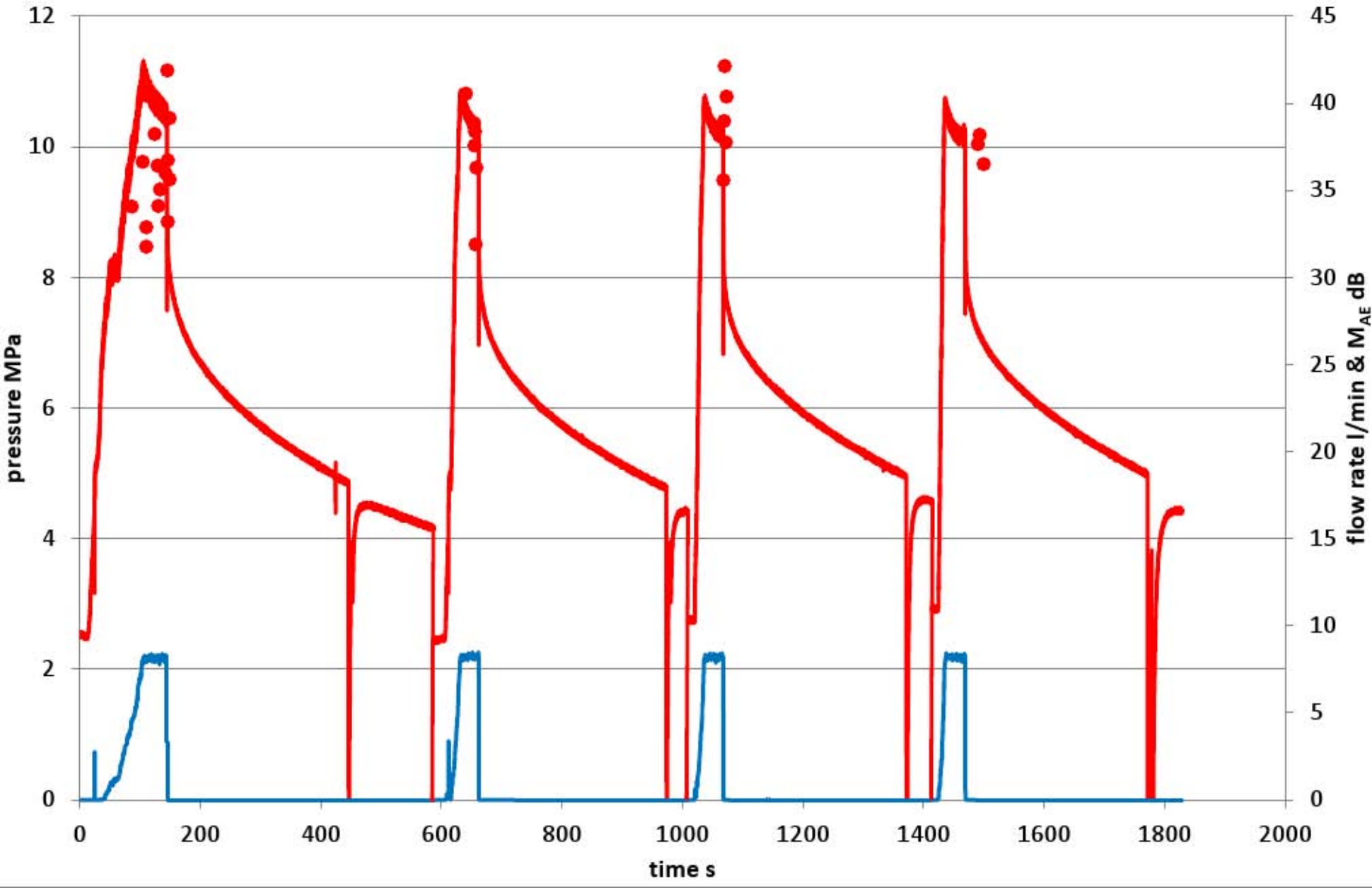
pressure MPa
flow rate l/min & M_{AE} dB
time s
0
2
4
6
8
10
12
0
5
10
15
20
25
30
35
40
45
0
200
400
600
800
1000
1200
1400
1600
1800
2000

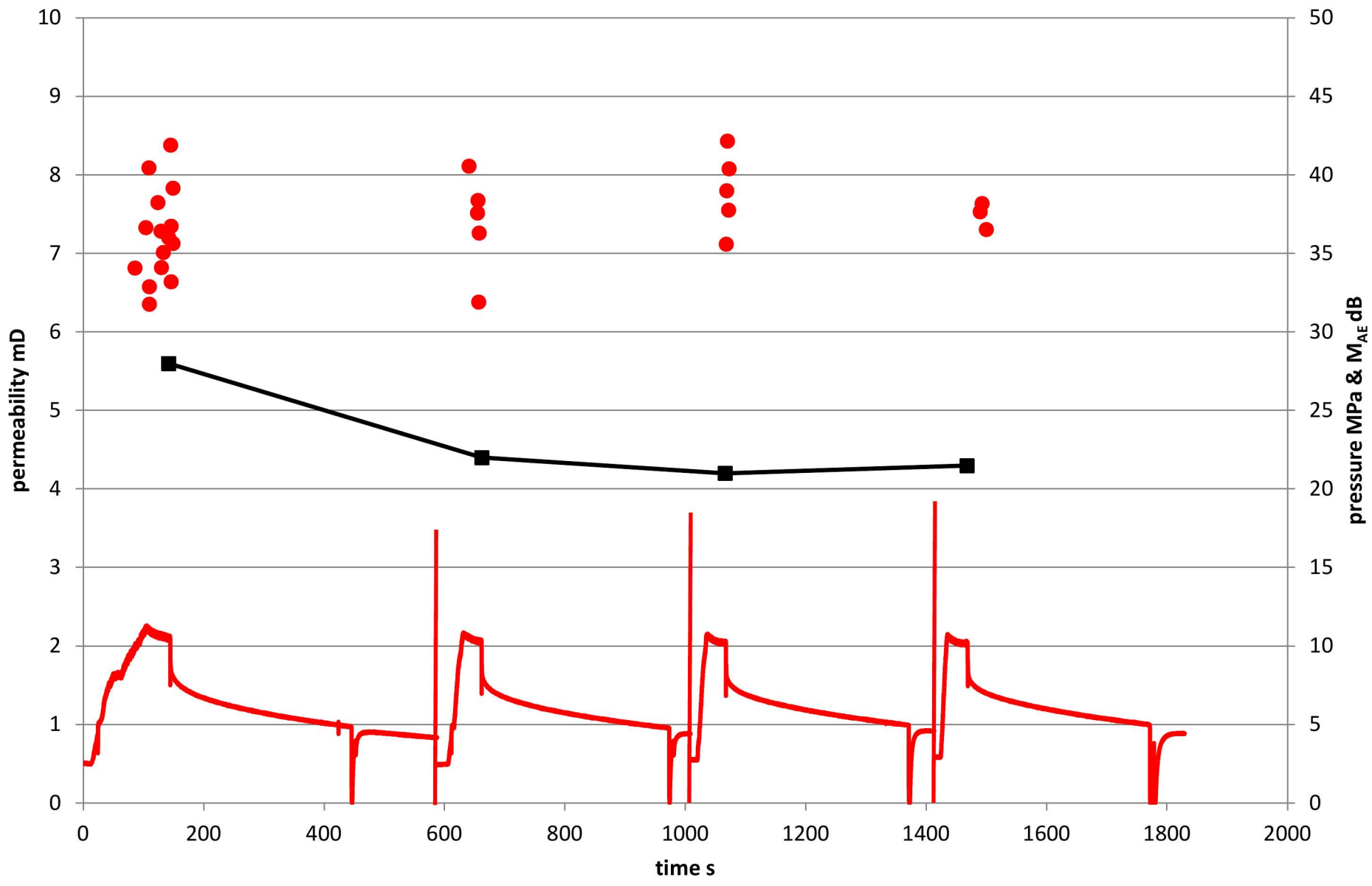
permeability mD
pressure MPa & M_{AE} dB
time s
0
1
2
3
4
5
6
7
8
9
10
0
5
10
15
20
25
30
35
40
45
50
0
200
400
600
800
1000
1200
1400
1600
1800
2000

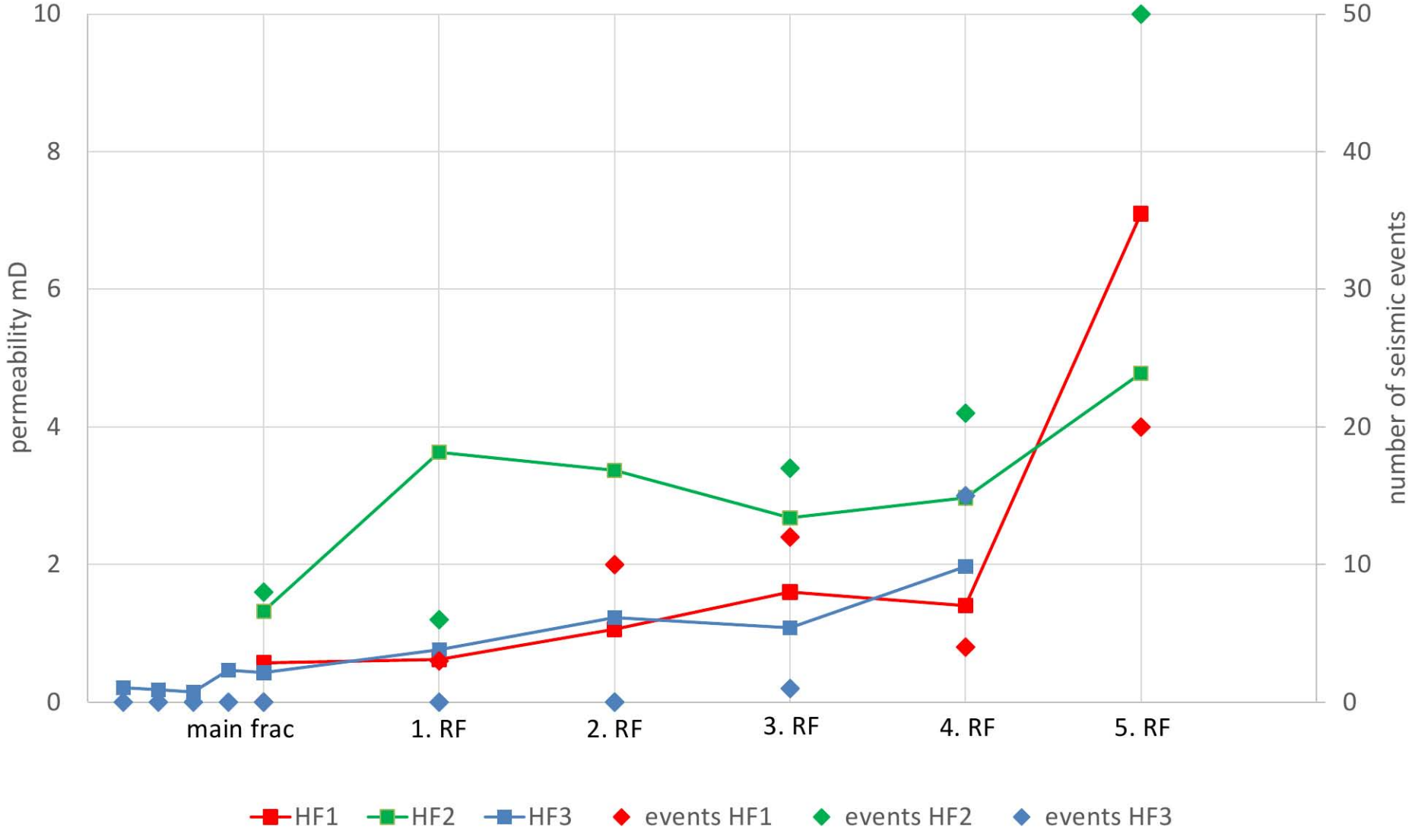
10
8
6
4
2
0
permeability mD
50
40
30
20
10
0
number of seismic events
main frac
1. RF
2. RF
3. RF
4. RF
5. RF
HF1
HF2
HF3
events HF1
events HF2
events HF3

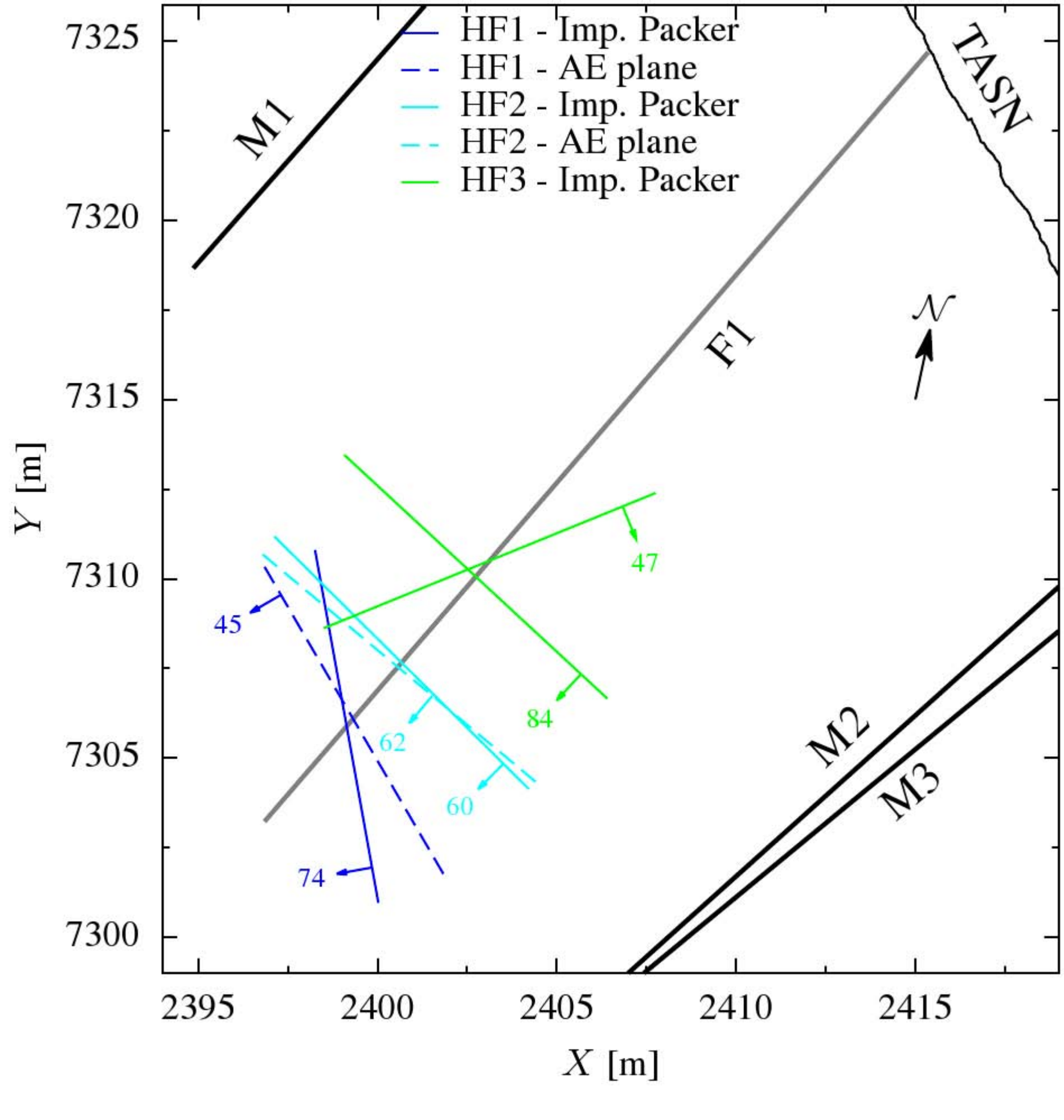
HF1 - Imp. Packer
HF1 - AE plane
HF2 - Imp. Packer
HF2 - AE plane
HF3 - Imp. Packer
M1
F1
TASN
M2
M3
N
45
74
62
60
84
47
7325
7320
7315
7310
7305
7300
Y [m]
2395
2400
2405
2410
2415
X [m]

Fracture trace	θ [deg]	β [deg]	α [deg]
HF1 A	153	243	74
HF2 A	118	208	60
HF3 A	051	141	47
HF3 B	116	206	84
HF4 A	177	087	85
HF4 B	083	353	63
HF4 C	147	237	89
HF4 D	129	219	77
HF5 A	068	158	49
HF6 A	127	217	80
HF6 B	067	157	54
HF6 C	145	055	71
HF6 D	121	211	62

Table B1 Orientations of fractures from impression packer tests (θ: fracture strike direction (North over East), β: dip direction (North over East), α: dip (with respect to horizontal))

Test at 25.0 m

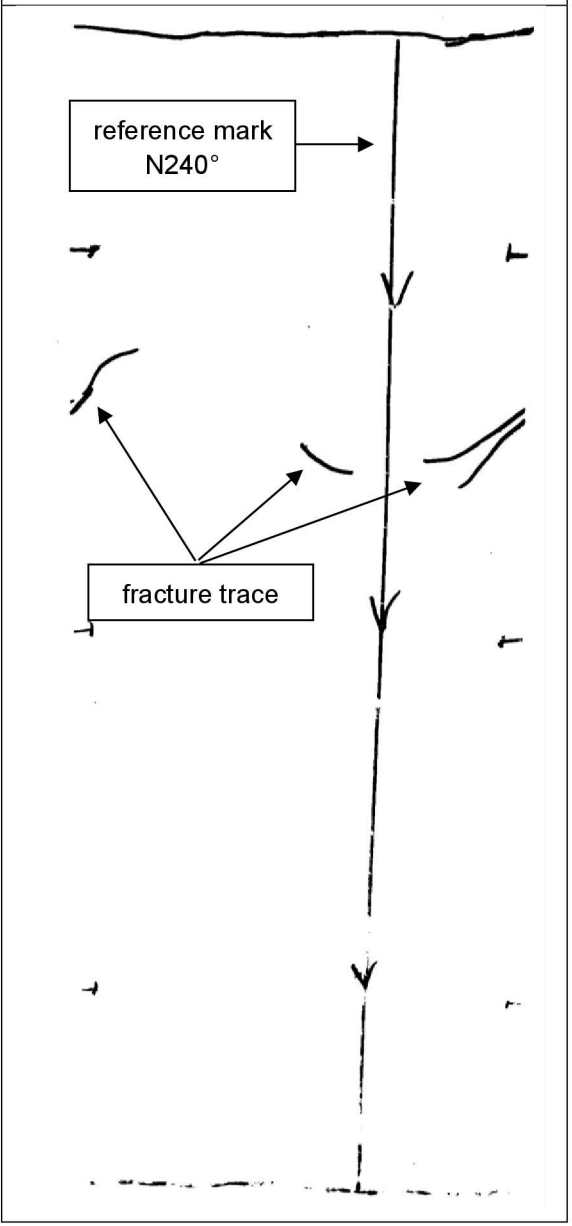

Test at 22.5 m

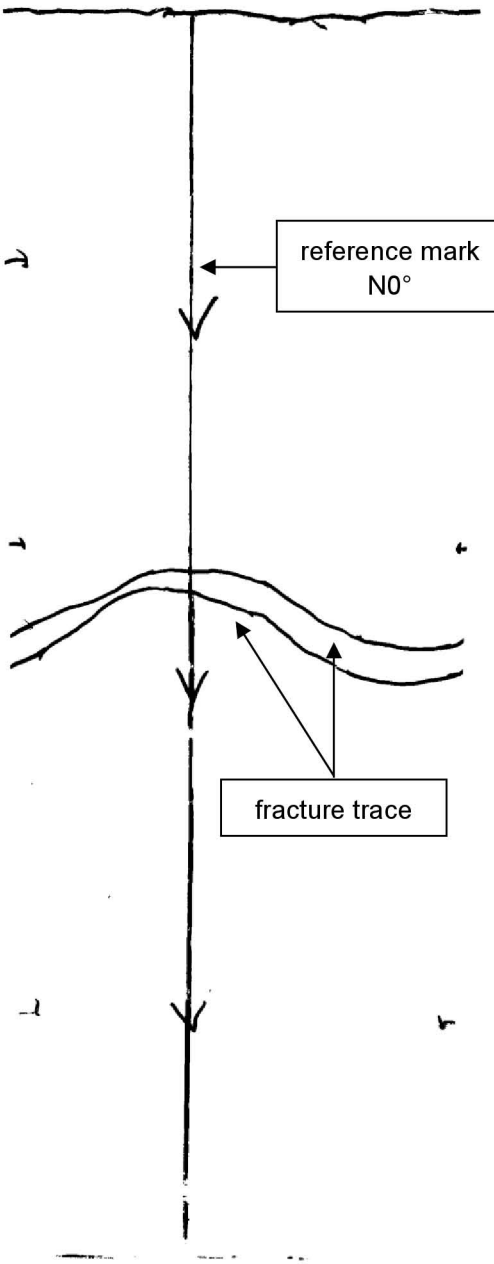

Test at 19.0 m

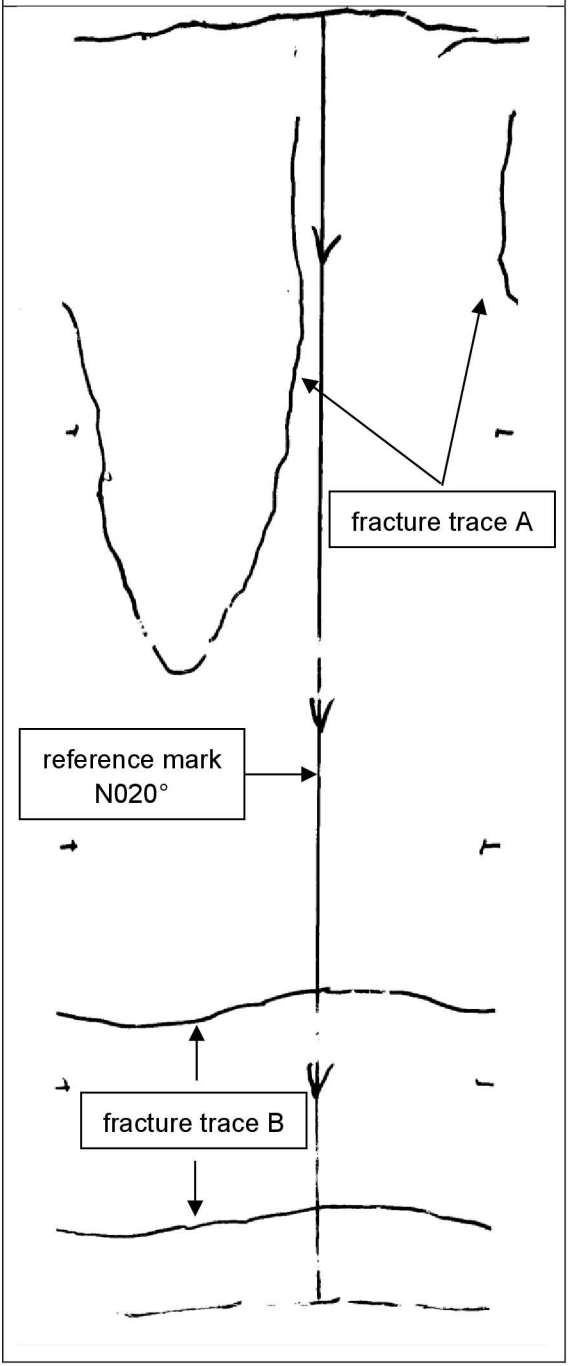

Test at 13.65 m

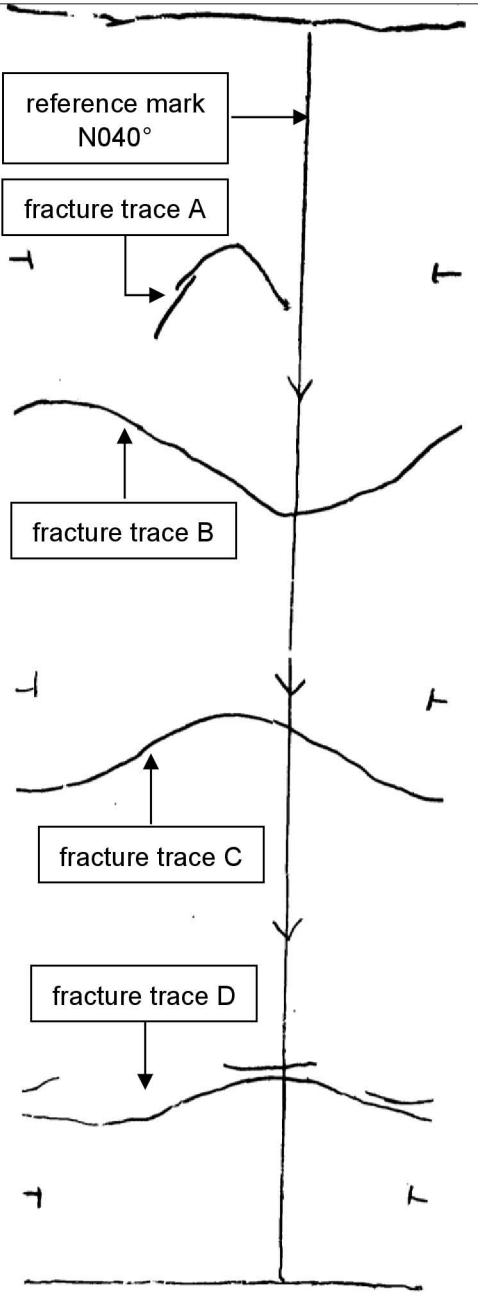

Test at 11.3 m

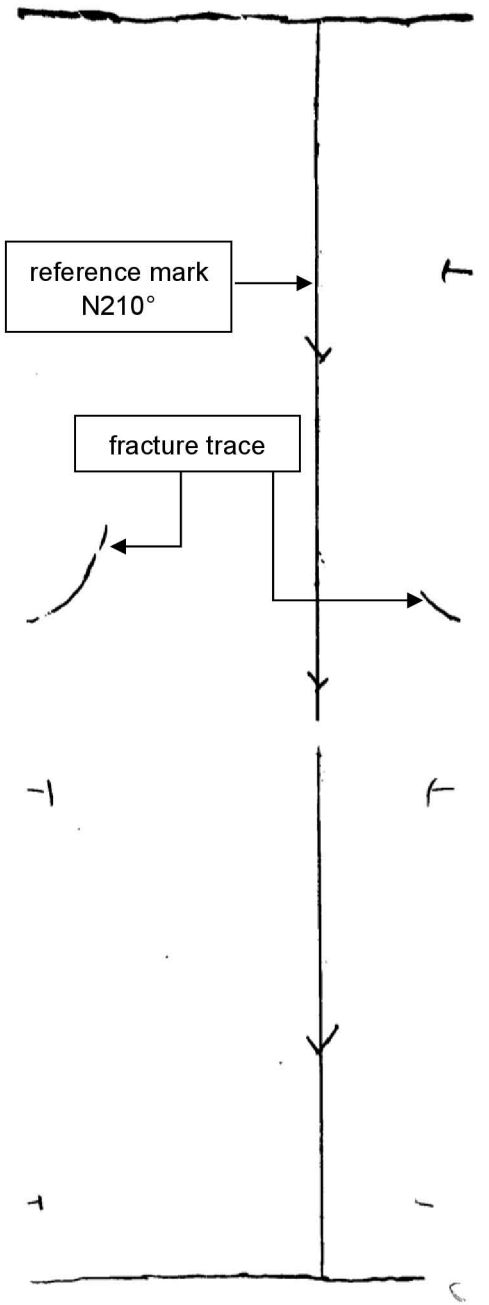

Test at 4.8 m

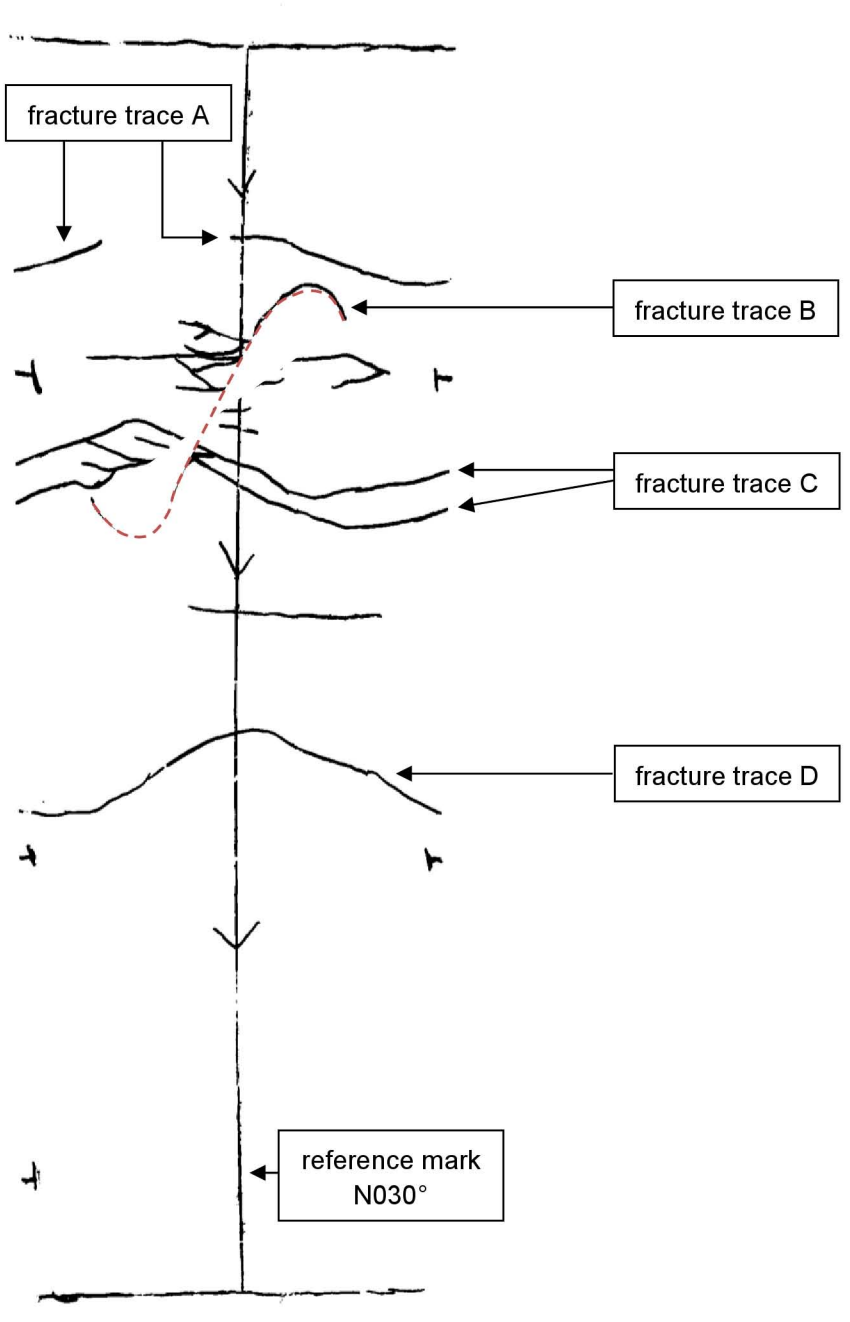
fracture trace A
fracture trace B
fracture trace C
fracture trace D
reference mark
N030°

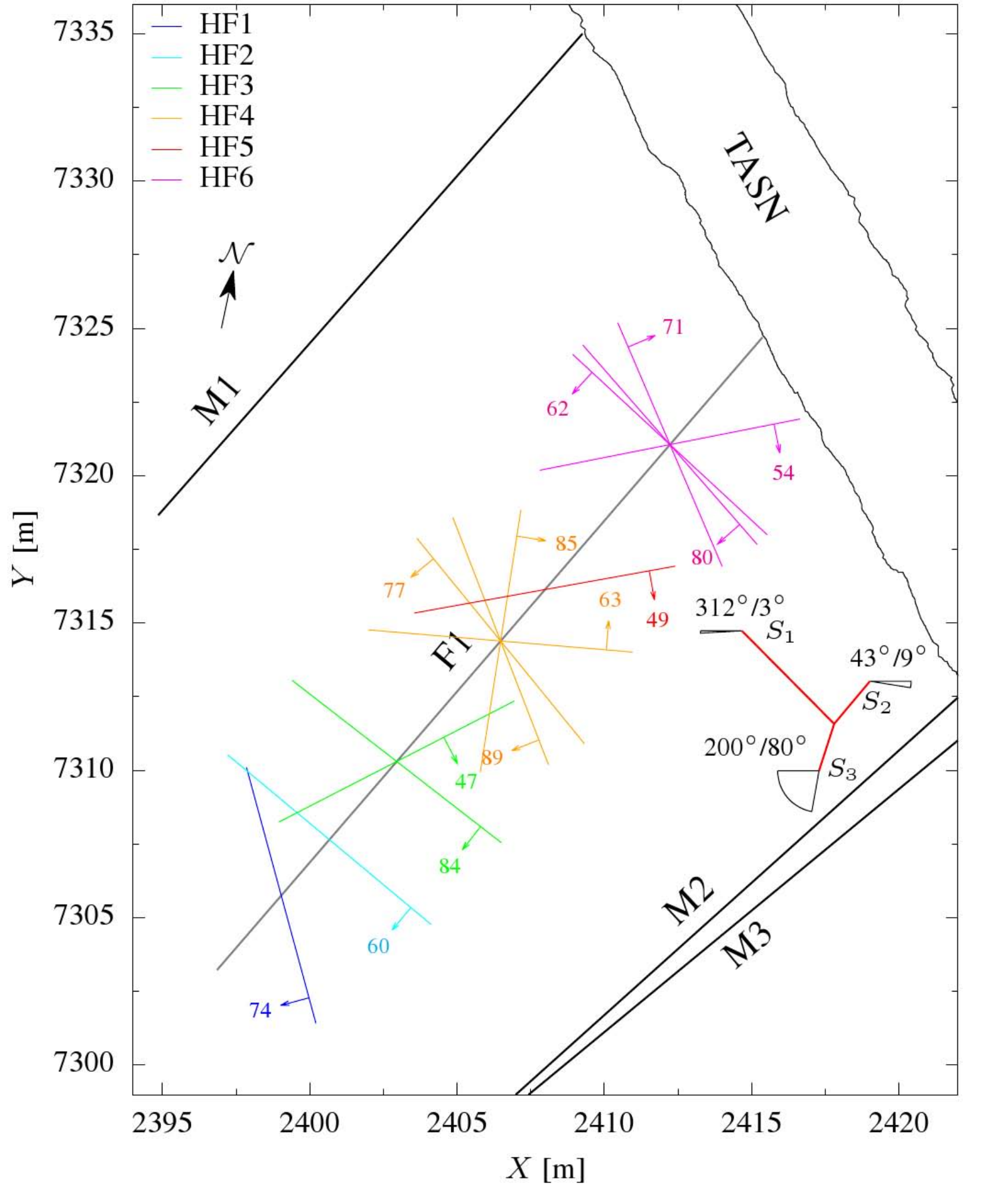
HF1
HF2
HF3
HF4
HF5
HF6
TASN
M1
M2
M3
F1
N
71
62
54
80
85
77
63
49
312°/3°
S_1
43°/9°
S_2
200°/80°
S_3
89
47
84
60
74
7335
7330
7325
7320
7315
7310
7305
7300
2395
2400
2405
2410
2415
2420
Y [m]
X [m]